Palaeogeography, Palaeoclimatology, Palaeoecology 663 (2025) 112779

Contents lists available at ScienceDirect

Palaeogeography, Palaeoclimatology, Palaeoecology

journal homepage: www.elsevier.com/locate/palaeo

Sea ice variability from the penultimate glacial to the last interglacial in the eastern Fram Strait

Kristine Steinsland [a,*], Danielle M. Grant [a,1], Kirsten Fahl [b], Ruediger Stein [b,c,d], Tine L. Rasmussen [e], Bjørg Risebrobakken [a], Ulysses S. Ninnemann [f], Jochen Knies [e,g], Julie Heggdal Velle [g], Stijn De Schepper [a]

[a] NORCE Climate and Environment and Bjerknes Centre for Climate Research, Bergen, Norway
[b] Alfred Wegener Institute Helmholtz Centre for Polar and Marine Research, Bremerhaven, Germany
[c] Faculty of Geosciences and MARUM Centre for Marine Environmental Sciences, University of Bremen, Bremen, Germany
[d] Frontiers Science Centre for Deep Ocean Multispheres and Earth System and Key Laboratory of Marine Chemistry Theory and Technology, Ocean University of China, Qingdao, China
[e] UiT The Arctic University of Norway, Tromsø, Norway
[f] University of Bergen and Bjerknes Centre for Climate Research Bergen, Norway
[g] Norwegian Geological Survey, Trondheim, Norway

ARTICLE INFO

Editor: M Elliot

Keywords:
Biomarkers
IP_{25}
Dinoflagellate cysts
Stable isotopes
Ice rafted debris
Western Svalbard margin

ABSTRACT

The ongoing reduction of Arctic sea ice underscores the need to understand the drivers behind sea ice variability and associated ocean-climate impacts. The Last Interglacial, Marine Isotope (sub)Stage (MIS) 5e, and its transitions offer insights into sea ice variability during a period warmer than pre-industrial, and intervals of large climatic changes. This study examines a marine sediment core from the eastern Fram Strait, covering late MIS 6 to early MIS 5b (140–90 ka). We analysed organic biomarkers, including the PIP_{25} sea ice index and dinoflagellate cyst assemblages, complemented by stable oxygen isotopes, total organic carbon, and sediment physical properties (ice rafted debris, X-ray fluorescence, magnetic susceptibility). Our findings demonstrate a progression from extensive sea ice cover during late MIS 6 to a marginal ice zone during Termination II (T II) and open ocean conditions during MIS 5e, influenced by the Svalbard–Barents Sea Ice Sheet (SBIS) and warm Atlantic surface waters, superimposed on the gradual changes in Northern Hemisphere summer insolation. During late MIS 6, intermittent local polynyas formed by katabatic winds and Atlantic water intrusions temporarily disrupted the sea ice cover. During T II, the marginal ice zone environment, combined with organic matter-rich meltwater influx from the retreating SBIS may have enhanced the biological pump. MIS 5e exhibited a "two-step" warming with the strongest influence of Atlantic waters around ~120 ka. Low to absent concentrations of biomarkers and dinoflagellate cysts immediately following MIS 5e complicate interpretations of sea ice and oceanic conditions during MIS 5d to MIS 5c, a crucial climatic interval characterised by periods with Northern Hemisphere summer insolation values comparable to today. These findings highlight the complexities of understanding Arctic sea ice responses to ocean-climate drivers and the need for further investigation into the unresolved MIS 5 proxy signals, important for improving our understanding of future sea ice decline and the associated ocean-climate impacts.

1. Introduction

Sea ice covers vast areas of the polar oceans and is a vital component in the Earth's climate system. In the Arctic, sea ice cover has steadily decreased over the last decades as atmospheric greenhouse gas concentrations have increased (Notz and Stroeve, 2016), and projections indicate sea ice-free Arctic summers within this century (Stroeve et al., 2007, 2012; Notz and Stroeve, 2018). This decrease has implications in and beyond the Arctic because sea ice affects the Earth's energy budget due to its high albedo, it influences ocean-atmosphere interactions, redistributes freshwater in the Arctic and subarctic marine environments, and hosts dynamic biogeochemical processes (e.g., Broecker, 1997; Hall,

* Corresponding author.
E-mail address: k.steinsland@uu.nl (K. Steinsland).
[1] Current address: Hakai Institute

https://doi.org/10.1016/j.palaeo.2025.112779
Received 7 February 2024; Received in revised form 7 January 2025; Accepted 26 January 2025
Available online 28 January 2025

2004; Dieckmann and Hellmer, 2008; Vancoppenolle et al., 2013).

Reconstructing sea ice variability during past time intervals that were warmer than during the pre-industrial Holocene can provide insights into future regional and global climate conditions and the impacts of an ice-free Arctic. One such period is the Last Interglacial, or Marine Isotope (sub)Stage (MIS) 5e, ca. 128–116 ka, when Arctic temperatures were 3–5 °C warmer than the pre-industrial Holocene (Jansen et al., 2007). Thus, MIS 5e is considered a good comparison for future climate, despite the MIS 5e warmth being paced under different orbital configurations than at present, where greenhouse gas concentrations drive much of the modern warming (Allen et al., 2018).

Today, there is no consensus on the sea ice conditions that existed in the Arctic Ocean during MIS 5e. Stein et al. (2017) presented biomarker records and modelling results that both showed extensive to perennial sea ice cover in the central Arctic Ocean throughout MIS 5e, while seasonally ice-free conditions occurred along the northern Barents Sea continental margin. More recently, a modelling study by Guarino et al. (2020) and a study based on the distribution of planktic foraminiferal species (Vermassen et al., 2023) suggest that the central Arctic Ocean during MIS 5e was seasonally (summer) sea ice-free during MIS 5e. Another controversy is whether the Arctic Ocean during the preceding glacial MIS 6 was covered by a massive thick floating ice shelf (Jakobsson et al., 2016; Geibert et al., 2021), whether it was covered with perennial sea ice (Stein et al., 2017) or was seasonally sea ice covered with multiple events of ice shelf expansion (Xiao et al., 2020). The discrepancies regarding the state of the Arctic Ocean highlight the need for further investigations, ideally using a multi-proxy approach on sediments from the same core. However, this is challenging due to difficulties in obtaining continuous sedimentary records with a reliable chronology and sufficient biogenic content that allows for detailed palaeoceanographic reconstructions (e.g., de Vernal et al., 2020a).

In our study, we investigated the sea ice variability and hydrography during late MIS 6 to 5b in the eastern Fram Strait, the Atlantic-Arctic gateway between Greenland and Svalbard (Fig. 1). This region is sensitive to the inflow and strength of northward-flowing Atlantic and southward-flowing Arctic waters, as well as to changes in ice sheet dynamics, which contribute to large environmental variability on glacial-interglacial timescales. Well-preserved sedimentary sequences in the Fram Strait provide valuable insights into sea ice variability in response to climate change in the wider Arctic Ocean region. Previous studies in this area have focused on reconstructing surface currents, ice sheet variability, and timing of warm climatic "optimum" conditions using proxies such as dinoflagellate cysts (hereafter dinocyst), foraminifers and sedimentological indices (e.g., Van Nieuwenhove et al., 2008, 2011; Matthiessen and Knies, 2001; Risebrobakken et al., 2006; Zhuravleva et al., 2017). While these proxies effectively indicate hydrographic conditions, they give mainly indirect information about sea ice (de Vernal et al., 2013). In contrast, the biomarker IP_{25}, synthesized by specific diatoms living in Arctic sea ice (Brown et al., 2014; Limoges et al., 2018a), serves as a direct and reliable indicator of past sea ice conditions (Belt et al., 2007; Fahl and Stein, 1997; Stein et al., 2012; Belt and Müller, 2013). Existing MIS 5e biomarker records from the Fram

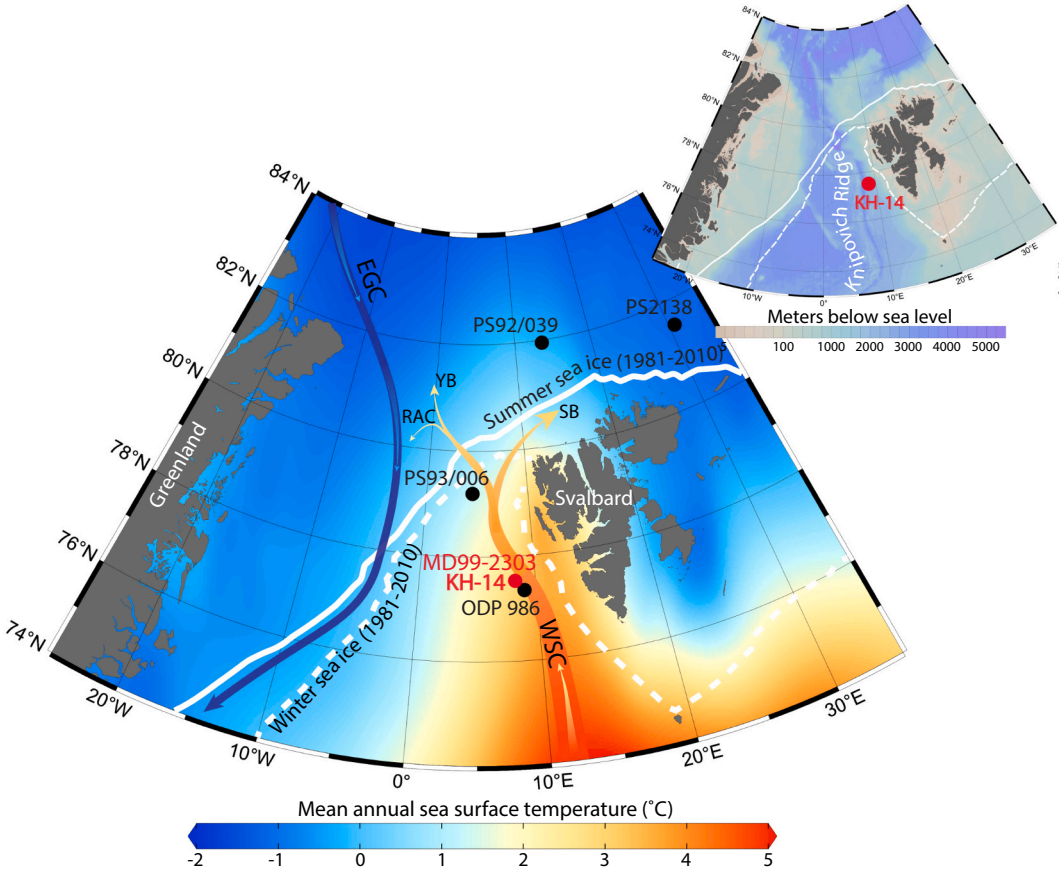

Fig. 1. Mean annual sea surface temperatures from WOA2018 (Locarnini et al., 2019) and major surface ocean currents relative to our studied core KH14-GPC02 (overlapping with MD99-2303; Risebrobakken et al., 2005, 2006) (red circle) and other core sites (black circles) discussed in the text. Western Spitsbergen Current (WSC), the East Greenland Current (EGC), Return Atlantic Current (RAC), Yermak Branch (YB), Svalbard Branch (SB), sea ice winter maximum (mean March 1981–2010) and sea ice summer minimum (mean September 1981–2010) extents are marked. Sea ice extent is from the National Snow and Ice Data Center (NSIDC), sea ice index, and the map was produced in Ocean Data View (Schlitzer, 2023). (For interpretation of the references to colour in this figure legend, the reader is referred to the web version of this article.)

Strait (Kremer et al., 2018a, 2018b; Stein et al., 2017, 2022) have shown that sea ice variability was closely linked to changes in the influence of Atlantic waters and the extent of the Svalbard–Barents Sea Ice Sheet (SBIS). However, these studies are limited by rather low resolution, particularly during the critical glacial-interglacial transitions when profound oceanic and cryospheric changes occurred.

We measured organic biomarkers (highly branched isoprenoids (HBIs), and sterols), stable oxygen isotopes, dinocyst assemblages, and sedimentological data (X-ray fluorescence, ice rafted debris, and magnetic susceptibility). With these methods, we reconstructed sea ice variability, extent and surface ocean hydrography across key climate transitions from late MIS 6, throughout Termination II (T II), MIS 5e and the ensuing MIS 5d to b. To contextualise our findings, we subsequently compared our data with other regional records, offering a comprehensive view of sea ice variability and the palaeoceanographic history of the Fram Strait (Fig. 1).

2. Regional setting

The Fram Strait is the only deep-water passage connecting the Arctic and North Atlantic oceans, regulating the exchange of water masses between them (Jakobsson et al., 2012; Haine et al., 2015). In the eastern Fram Strait, the northward-flowing West Spitsbergen Current (WSC) (Fig. 1) carries warm and saline Atlantic waters along the continental margin of Svalbard into the Arctic Ocean as the northernmost continuation of the North Atlantic Current (NAC) (Aagaard, 1982; Schauer et al., 2004). Between 78 and 80°N the WSC splits into a westward flowing Return Atlantic Current (RAC), a north-eastward flowing Svalbard branch (SB), and a northward flowing Yermak Branch (YB) (Bourke et al., 1988; Manley, 1995; Hattermann et al., 2016). In the western Fram Strait, the East Greenland Current (EGC) flows southward from the Arctic Ocean along Greenland, transporting polar freshwater and sea ice (Aagaard and Coachman, 1968; Vinje, 2001; Rudels et al., 2002). Between the EGC and WSC lies the Arctic domain, a region of mixed water masses bordered by the Polar Front to the west and the Arctic Front to the east.

Until recently (1981–2010), the ocean surrounding the Svalbard archipelago was covered by winter sea ice (Fig. 1), but lately, sea ice has declined to near ice-free year-round conditions in the eastern Fram Strait and ice-free areas north of Svalbard (Polyakov et al., 2017). The northward retreat of sea ice, with attendant reductions in stratification, increased vertical mixing, and altered primary production is known as “atlantification” (Reigstad et al., 2002; Ingvaldsen et al., 2021), and has been linked to a contemporary increase in the temperature of the Atlantic water inflow (Ivanov et al., 2012; Onarheim et al., 2014).

3. Materials and methods

Sediment core CAGE19-3-KH14-GPC02 (hereafter KH-14) was recovered in 2019 by R/V Kronprins Haakon from the Fram Strait (77° 31’ 22.7994″ N, 8° 24’ 4.9674″ E, 2275 m below sea level), near the location of core MD99-2303 (77° 31’ 10.8006″ N, 8° 23’ 58.8012″ E, 2325 m below sea level), where Risebrobakken et al. (2005, 2006) identified MIS 5e. The studied core interval consists of homogenous silty clay, with variations in silt content and dropstones across different intervals, evident from the initial core description (Supplementary Fig. 1): increased silt and frequent dropstones (>2 mm) between 658 and 568 cm, considerably finer sediments with little or very fine silt in clay between 568 and 528 cm, and a return to higher silt content and increased number of dropstones between 528 and 458 cm. For the interval ca. 590–510 cm, samples were taken every 0.5 cm for ice rafted debris (IRD; grains >0.5 mm) and stable oxygen isotope analyses ($\delta^{18}O$), every 1 cm for biomarker and total organic carbon (TOC) analyses, and every 2 cm for dinocyst analyses. In the surrounding intervals (658–590 and 510–458), samples were taken every 1 cm for IRD and $\delta^{18}O$ analyses, every 2 cm for biomarker and TOC analyses, and every 4 cm for dinocyst analyses.

In total, 200 samples were taken from the core sections (458–658 cm) for $\delta^{18}O$ and IRD analysis. The samples (wet) weighed on average 19 ± 4 g (1σ), were freeze-dried and re-weighed before being wet-sieved over mesh-sizes 0.5, 0.1, and 0.063 mm. The size fraction 0.1–0.5 mm was picked for planktic foraminiferal species *Neogloboquadrina pachyderma* and benthic foraminiferal species *Cibicidoides wuellerstorfi* and *Oridorsalis umbonatus*, to be used for $\delta^{18}O$ analyses. Due to a low abundance of foraminifera, not all intervals could be analysed. A Finnigan MAT253 mass spectrometer with an online Kiel IV, located at FARLAB, University of Bergen, was used for the $\delta^{18}O$ analyses. Values are reported relative to Vienna Pee Dee Belemnite (VPDB). Two working standards (CM12 and Riedel) and two international standards (NBS-18 and NBS-19) were analysed with the samples. The external precision for samples between 15 and 100 μg was better than 0.08 ‰ for $\delta^{18}O$, based on the long-term reproducibility (1σ) of the working standard CM12. Mineral grains representing IRD were picked and counted from the 200 samples in the size fraction >0.5 mm and are presented as the number of grains per gram dry weight sediment.

TOC (%) was measured on 100 mg of freeze-dried and homogenized sediments (per sample) using an ELTRA CS2000 Carbon Sulfur Detector. 133 samples were measured at the Alfred Wegener Institute Helmholtz Centre for Polar and Marine Research.

The volume low-field magnetic susceptibility (k) was measured on u-channels in 3 mm increments at the Geological Survey of Norway (NGU) in Trondheim using a GEOTEK MSCL-S core logger equipped with a Bartington MS3 and a loop sensor of diameter 60 mm.

X-Ray fluorescence (XRF) core logging was carried out with the Standard MSCL (MSCL-S) core logger (GeoTek Ltd., UK) and an attached DELTA Handheld XRF sensor. The XRF sensor was equipped with a 4-W Rh Tube anode and Si drift detector. Before core measurements, the XRF sensor was standardized and SRM 2710a Montana soil I standard sample was stationary measured for sensor-control purposes. Downcore XRF measurements were taken incrementally along the longest axis in the centre of the split core surfaces with 0.5 cm steps. Two measurements in succession with 40 keV and 10 keV currents and 10 s exposure time each provided spectra covering chemical elements, of which Ca and Ti concentrations (ppm) were used for this study.

3.1. Palynological analyses and general interpretation

In total, 70 samples (ca. 15 g average dry weight per sample) were analysed for dinocyst assemblages following a standard palynological preparation procedure (e.g., De Schepper et al., 2017). Room-temperaure hydrochloric (50 % HCl) and hydrofluoric (60 % HF) acids were added to remove the mineral fraction. HCl was added until the sample stopped reacting, and HF was added and left for two days with periodic stirring. The palynological residue was sieved over a 10 μm polymer mesh and mounted on microscope slides with glycerine jelly. To calculate the dinocyst concentrations and their associated errors (Stockmarr, 1971), one tablet of *Lycopodium clavatum* spores (batch #140119321, n = 19,855 ± 521 spores per tablet) was added to each sample before chemical treatment. Slides were prepared at the Palynological Laboratory Services (Wales, UK). Dinocyst assemblages were counted at ×400 magnification until a minimum of 300 in situ dinocysts were identified. The entire slide (ca. 20 non-overlapping traverses) was counted if the concentration was too low to reach this threshold.

Dinocyst taxonomy and nomenclature followed Van Nieuwenhove et al. (2020) and Fensome et al. (2019) (DINOFLAJ3). *Brigantedinium* specimens, classified only when an intercalary (2a) archeopyle could be observed, were grouped with other round brown cysts (RBC) that could not be identified to genus level due to folding or orientation. Of the spiniferate dinocysts the cool-water *S. elongatus* and warm-water *S. mirabilis* were identified, while the *Spiniferites* spp. group consists of *S. ramosus* and specimens that could not be identified to species level. All *Impagidinium* species were grouped as *Impagidinium* spp. (*I. aculeatum, I.*

sphaericum, I. paradoxum) because of their very low counts (ca. 1 per sample where present) except for *Impagidinium pallidum,* due to its distinct cool environmental preferences and notably higher counts.

Dinoflagellate distribution in the surface ocean is influenced by physical and chemical parameters such as currents, temperature, salinity, irradiance, turbulence, nutrients and sea ice (e.g., de Vernal et al., 2020b). Approximately 15–20 % of dinoflagellates are known to produce organic-walled cysts (Head, 1996), which are well-studied proxies for upper water mass properties in the northern latitudes (e.g., Rochon et al., 1999; Marret et al., 2004; Matthiessen et al., 2005; Zonneveld et al., 2013; de Vernal et al., 2020b). In modern North Atlantic sediments, *Operculodinium centrocarpum* sensu Wall and Dale (1966) (hereafter *O. centrocarpum*), is commonly associated with Atlantic waters, making it a key indicator for interglacial intervals with warm Atlantic waters in the fossil record (e.g., Harland, 1983; Rochon et al., 1999; Matthiessen et al., 2001; Matthiessen and Knies, 2001; Grøsfjeld et al., 2006; de Vernal et al., 2020b). *Nematosphaeropsis labyrinthus*, a subpolar-temperate species (Rochon et al., 1999; Marret and Zonneveld, 2003), has been associated with climate transitions, particularly during glacial-interglacial intervals (Hennissen et al., 2017, and references therein). In polar to subpolar regions, *Islandinium minutum* is characteristic of cooler surface ocean conditions and seasonal sea ice (de Vernal et al., 2020b), while *Imagidinium pallidum* is typically found in the cold, open ocean of the Arctic water domain, between the EGC and WSC (Marret and Zonneveld, 2003). The RBCs, a group of heterotrophic taxa, are associated with the trophic state of the surface waters, in addition to temperature and salinity. Thus, in environments with increased nutrient availability, such as frontal zones and sea ice margins, RBCs and other heterotrophic dinocyst taxa commonly outnumber other dinocysts (e.g., de Vernal et al., 2020b).

3.2. Biomarker analyses and general interpretation

In total, 133 samples were analysed for biomarkers (HBIs and sterols). In preparation for the analyses, 5 g of freeze-dried sediment was homogenized using an agate mortar. Before extraction, the internal standards 7-hexylnonadecane (7-HND: 0.076 µg/sample), 5α-androstan-3β-ol (androstanol, 10.6 µg/sample), 9-octylheptadec-8-ene (9-OHD: 0.1 µg/sample), and squalane (3.2 µg/sample) were added to the sediments to allow quantification or routine methodical checks. Biomarkers were extracted by sonication (3 × 15 min) using dichloromethane: methanol (2:1 *v*/v; 30 ml) as solvent. The extract was separated into hydrocarbon and sterol fractions through open-column chromatography (5 ml *n*-hexane for hydrocarbons and 9 ml ethylacetate:*n*-hexane (4:1) for sterols) with silica gel (SiO_2) as the stationary phase. The sterol fraction was silyated with 200 µl BSTFA (bis-trimethylsilyl-trifluoracetamide; 60 °C for 2 h).

Biomarker analyses were performed by gas chromatography-mass-spectrometry (GC–MS). Hydrocarbon concentrations were determined with an Agilent Technologies 7890 gas chromatograph (30 m DB-1MS column, 0.25 mm in diameter and 0.25 µm film thickness) coupled to an Agilent Technologies 5977 A mass selective detector. Sterol concentrations were measured with an Agilent Technologies 6850 gas chromatograph (30 m DB-1MS column, 0.25 mm in diameter and 0.25 µm film thickness) coupled to an Agilent Technologies 5975 A mass selective detector. The HBI (IP_{25}) and the sterols were identified by comparing their retention times to those of reference compounds (IP_{25}: Belt et al., 2007; sterols: Boon et al., 1979; Volkman, 1986). IP_{25} (*m/z* 350) was quantified by the abundant fragment ion m/z 266 of the internal standard 7-HND. Sterols were quantified as trimethylsilyl ethers (brassicasterol: m/z 470, campesterol: m/z 472, sitosterol: m/z 486, dinosterol: m/z 500) relative to the molecular ion of androstanol (m/z 348). The different responses of all these ions were balanced by external calibration. Instrument stability was controlled by reruns of external standards and replicate analyses for random samples. All biomarker concentrations have been normalised to the TOC to compensate for dilution effects caused by variations in sedimentation rates.

The molecular biomarker IP_{25} (Ice Proxy with 25 carbon atoms) is synthesized by a relatively limited number of diatoms (namely *Pleurosigma stuxbergii* var. *rhomboides*, *Haslea crucigeroides* (and/or *Haslea spicula*), and *Haslea kjellmanii*) residing in the base of Arctic sea ice (Brown et al., 2014; Limoges et al., 2018a), primarily in regions characterised by seasonal sea ice (Belt et al., 2007; Xiao et al., 2015; Kolling et al., 2020; for review see Belt, 2018). The presence of IP_{25} reliably indicates seasonal sea ice, while its absence may reflect either permanent sea ice due to limited light and nutrient availability which are required for the growth of sea ice diatoms, or open-water environments where the sea ice habitat is absent. To distinguish between these environments, it requires that IP_{25} is analysed alongside biomarkers associated with open waters such as brassicasterol and dinosterol (e.g., Müller et al., 2011; Müller et al., 2009), which are produced by various phytoplankton including dinoflagellates, diatoms, and haptophytes (Boon et al., 1979; Robinson et al., 1984; Volkman et al., 1998). As an approach to address the challenge of misjudging absent IP_{25} either reflecting perennial ice cover or ice-free waters, the PIP_{25} index was developed (Müller et al., 2011). This semi-quantitative measure combines IP_{25} with the open-water phytoplankton biomarker brassicasterol (P_BIP_{25}) and dinosterol (P_DIP_{25}).

$$PIP_{25} = IP_{25}/(IP_{25} + (\text{phytoplankton biomarker}^{*}c)\,).$$

The balance factor *c* is included to counterbalance the naturally higher concentrations of the sterols compared to IP_{25}.

c = mean IP_{25} concentration/mean phytoplankton biomarker concentration.

Both P_BIP_{25} and P_DIP_{25} indices have been shown to have a positive correlation with modern satellite-based sea ice observations (e.g., Müller et al., 2012; Xiao et al., 2015; Kolling et al., 2020). Following Müller et al. (2011), high PIP_{25} index values (0.75–1.00) reflect extensive to perennial (1.00) sea ice cover, intermediate values (0.50–0.75) refer to seasonal ice cover or a stable ice edge, while low values (0.00–0.50) indicate little to ice-free conditions. Alongside the PIP_{25} values, it is equally important to consider the individual biomarker concentrations to distinguish different sea ice conditions (Müller et al., 2011).

4. Results

4.1. Chronology and stable oxygen isotopes

The chronology of core KH-14 was established by correlating its sediment physical properties with those of the nearby core MD99-2303 (located ~400 m away), for which Risebrobakken et al. (2005, 2006) established an age model (Fig. 2). Initial correlation of magnetic susceptibility between KH-14 and MD99-2303 suggested that MIS 5e would occur between ~458–658 cm in KH-14, leading to the focus on this interval. We refined the identification of MIS 5e by correlating Ca-XRF

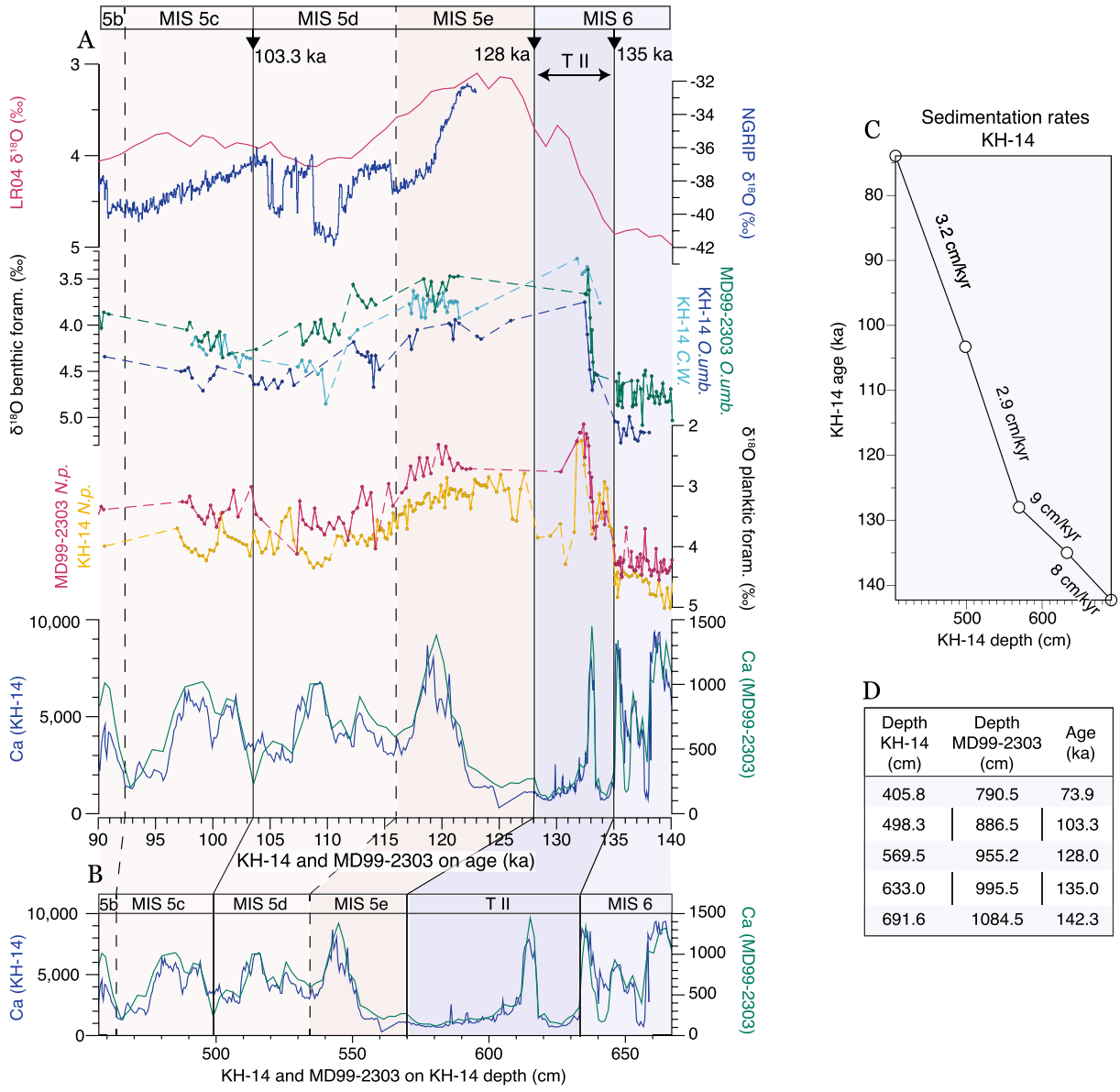

Depth KH-14 (cm)	Depth MD99-2303 (cm)	Age (ka)
405.8	790.5	73.9
498.3	886.5	103.3
569.5	955.2	128.0
633.0	995.5	135.0
691.6	1084.5	142.3

Fig. 2. Chronology for core KH-14 and correlation with MD99-2303 (Risebrobakken et al., 2005, 2006). A) The global benthic foraminiferal $\delta^{18}O$ LR04 stack (Lisiecki and Raymo, 2005), and the NGRIP ice core from Greenland for reference (NGRIP community members, 2004), KH-14 and MD99-2303 benthic oxygen isotopes (*C. wuellerstorfi* and *O. umbonatus)* and planktic oxygen isotopes (*N pachyderma)*, and Ca (counts) plotted on the KH-14 age scale based on tie point ages from Risebrobakken et al. (2005, 2006), B) alignment of Ca (counts) between KH-14 and MD99-2303 on KH-14 depth (cm below seafloor), C) sedimentation rates for KH-14, D) tie points with ages between KH-14 and MD99-2303 based on the Ca-XRF correlation used to align KH-14 and MD99-2303. Ca-XRF from MD99-2303 is partly published in Risebrobakken et al. (2006) and partly made available by Thomas Richter (personal communication).

data from KH-14 with MD99-2303, which revealed clear patterns that could be correlated between the two sites (Fig. 2A, B). Secondly, the benthic and planktic foraminiferal $\delta^{18}O$ were utilized to identify the glacial-interglacial transitions. We created the age model for KH-14 using five tie points (Fig. 2D) based on MD99-2303 (Risebrobakken et al., 2005, 2006), and then updated the ages of the major climate transitions to that of the MD95-2042 "Shackleton" ages (Shackleton et al., 2002, 2003).

The stratigraphic positions of the MIS 6–T II and T II–MIS 5e transitions in MD99-2303 were updated based on new data from KH-14, refining the original age model by Risebrobakken et al. (2005, 2006). The ages of these transitions were assigned according to the Shackleton et al. (2002, 2003) determination of MIS 5e. We note that T II falls within the late MIS 6 nomenclature (cf. Railsback et al., 2015), and we refer to the original MIS 6/5 transition as the T II/MIS 5e transition hereafter. The onset of T II (135 ka) was placed at 633 cm depth in KH-14, corresponding to a decrease in $\delta^{18}O$ of the benthic foraminifer *O. umbonatus* (Fig. 2A). Above this decrease, a large interval with nearly absent benthic foraminifers between ~610 and 550 cm (~132–121 ka) introduced uncertainty in defining climatic transitions. Likewise, planktic foraminifers were scarce within this interval, especially between ~600 and 572 cm (~131–128 ka). Despite this, we set the T II–MIS 5e boundary (128 ka) at ~569.5 cm, where a decrease in planktic $\delta^{18}O$ occurred. In MD99-2303, this boundary was positioned higher due to the later reappearance of planktic foraminifers compared to KH-14. For the remaining tie points, the original allocations in core MD99-2303 of Risebrobakken et al. (2005) were kept and transferred to core KH-14 based on the Ca-XRF correlation. This includes a tie point at 498.3 cm core depth, approximately at the start of the interstadial MIS 5c (103.3 ka), and tie points at 405.8 cm (73.9 ka) and 691.6 cm (142.3 ka) to further constrain sedimentation rates beyond MIS 5c and MIS 6 (see Fig. 2D for details).

4.2. Ice rafted debris

T II (135–128 ka) is characterised by high and variable IRD concentrations (Fig. 4H). IRD drops to zero shortly after the transition into MIS 5e and remains low until late MIS 5e, where it peaks shortly at 118 ka. Following MIS 5e, IRD concentrations remain relatively low until the periods centred around 104 and 94 ka when IRD increases to approximately 60 grains/g sediment.

4.3. Total organic carbon, magnetic susceptibility, and XRF-Ca/Ti

During late MIS 6, XRF-Ca/Ti is generally high but characterised by abrupt variability (Fig. 4F), closely mirroring changes in magnetic susceptibility (Fig. 4G). In contrast, TOC follows an antiphase pattern (Fig. 4E). At the onset of T II, TOC is high while Ca/Ti and magnetic susceptibility are low. TOC then declines sharply as Ca/Ti rises, followed by an increase after 133 ka, coinciding with another Ca/Ti decrease. TOC declines into MIS 5e, and remains low throughout the interglacial. Ca/Ti also remains low in early MIS 5e but rises substantially in the late phase, peaking between 121 and 119 ka. Magnetic susceptibility increases in early MIS 5e but declines around 125 ka. During MIS 5d–c, TOC and Ca/Ti exhibit substantial variability, maintaining the antiphase relationship observed in MIS 6 and T II.

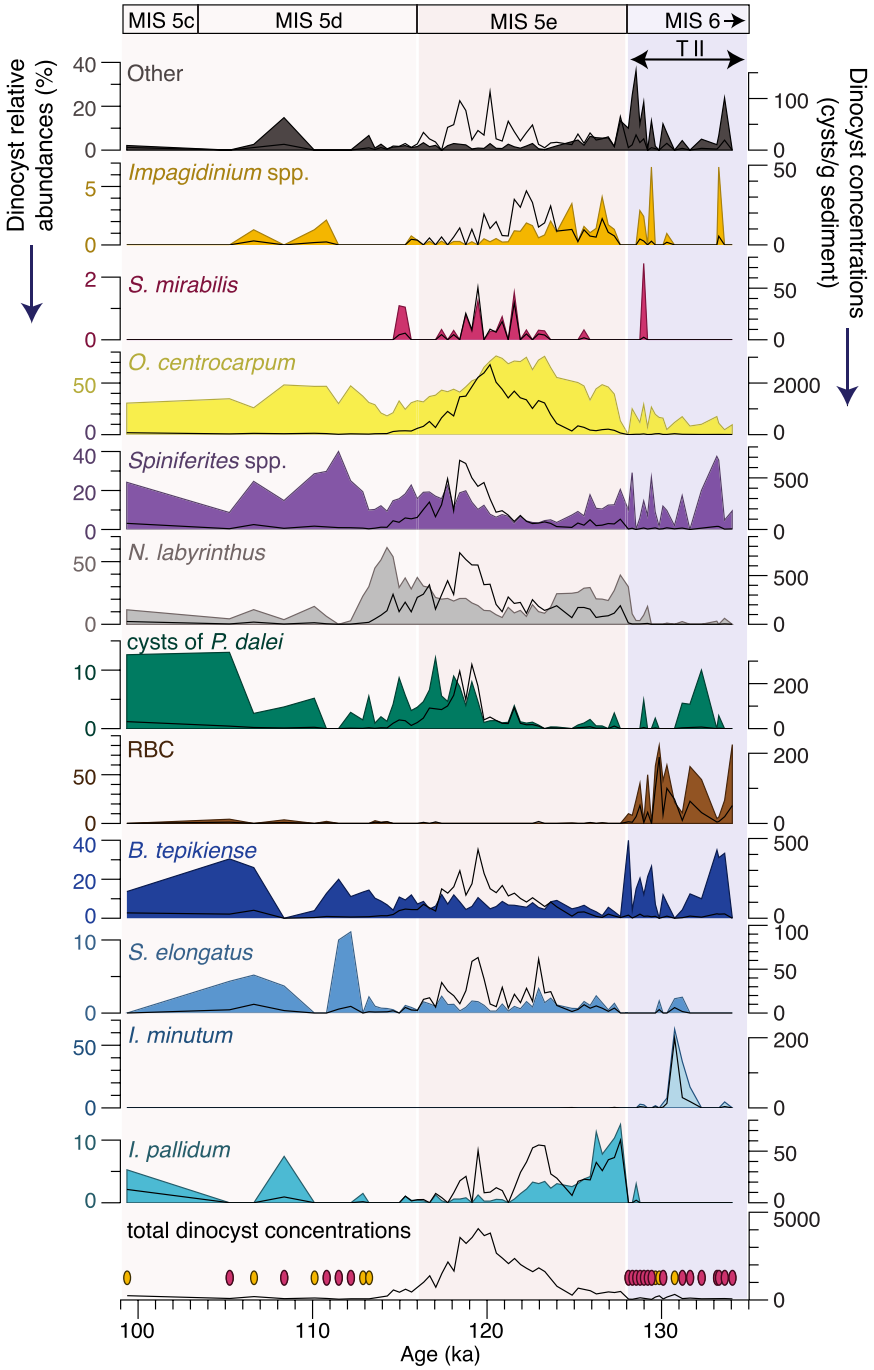

Fig. 3. Dinocyst relative abundances (coloured shaded areas) and concentrations (lines) for the most abundant species, and the total dinocyst concentrations. Samples where <100 specimens (orange) and <50 specimens (red) were counted are marked by the ovals in the lower panel. (For interpretation of the references to colour in this figure legend, the reader is referred to the web version of this article.)

4.4. Dinoflagellate cysts

A total of 19 dinocyst taxa were identified, with peak concentrations at ca. 120 ka, reaching up to 4000 cysts/g sediment (Fig. 3). In early MIS 5e (128–123 ka) concentrations were lower, averaging 500 cysts/g sediment, compared to an average of 2300 cysts/g sediment during late MIS 5e (123–116 ka). The lowest concentrations were recorded during T II and MIS 5d–c, averaging around 100 cysts/g sediment.

The most abundant dinocyst taxa are *O. centrocarpum*, *N. labyrinthus, Spiniferites* spp., and the RBCs (Fig. 3). During T II (135–128 ka), heterotrophic RBCs generally dominate the dinocyst assemblage, followed by *B. tepikiense* and *Spiniferites* spp. The sea ice associated *I. minutum* is dominant in one sample at 131 ka in T II. At the onset of MIS 5e (128 ka), the RBCs disappear and *I. pallidum* emerges as a distinctive species with coupled high abundance and concentration unique to this period. Throughout MIS 5e, *O. centrocarpum* is the most dominant species with a marked concentration increase from ca. 124 ka. *N. labyrinthus* and *Spiniferites* spp. make up the second and third most abundant taxa.

Early MIS 5d is characterised by a peak in *N. labyrinthus* abundance, coinciding with a decline in total dinocyst concentrations to an average of ca. 420 cysts/g sediment (116–114), and further decreasing to ca. 100 cysts/g sediment after 114 ka. The most abundant taxa during the remainder of MIS 5d are *O. centrocarpum*, *Spiniferites* spp., cysts of *P. dalei* and *B. tepikiense*. However, a word of caution is necessary for making environmental interpretations because the concentrations are low and few specimens (average of 55) per slide could be counted

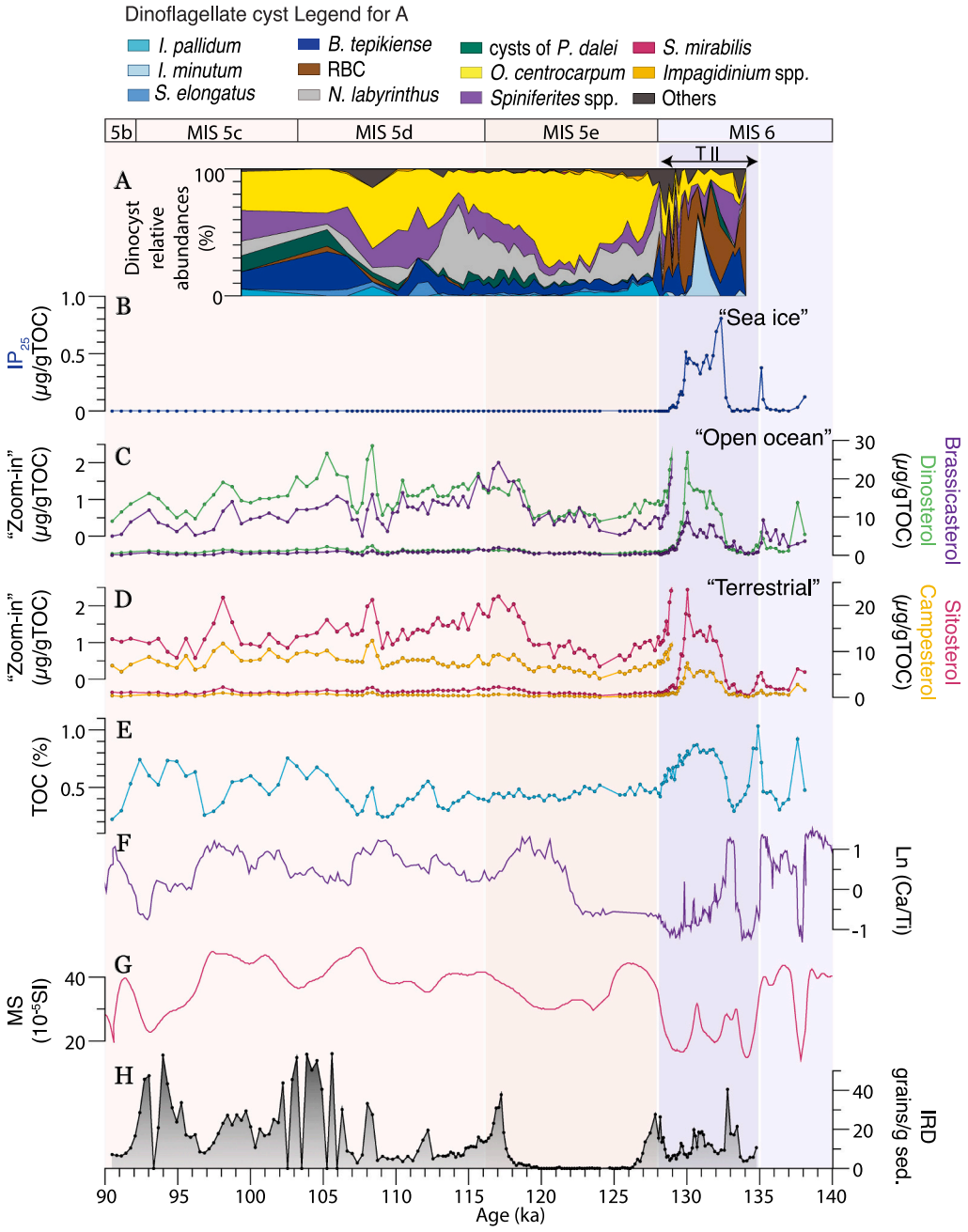

Fig. 4. Proxy data from KH-14. A) Dinocyst relative abundances with the most abundant taxa, B) concentrations of sea ice biomarkers IP_{25}, C) concentrations of open ocean phytoplankton biomarkers brassicasterol and dinosterol and a "zoom-in" of their concentrations from MIS 5e–b, D) concentrations of terrestrial biomarkers sitosterol and campesterol and a "zoom-in" of their concentrations from MIS 5e–b, E) total organic carbon (TOC) %, F) Ln (Ca/Ti)-element XRF G) magnetic susceptibility (MS), H) ice rafted debris (IRD).

between 114 and 90 ka. Such low counts lead to substantial uncertainty in the relative abundances (e.g., Heslop et al., 2011) and hamper environmental interpretations.

4.5. Biomarkers

Sea ice biomarkers (IP_{25}) are present in low concentrations in late MIS 6 (135–140 ka) (Fig. 4B). Here, moderate concentrations of the open ocean biomarkers (dinosterol and brassicasterol) and terrestrial biomarkers (sitosterol and campesterol) also occur (Fig. 4D, E). In early T II (133–135 ka), all biomarker concentrations decrease substantially, with IP_{25} detectable in only about half the samples. From 133 ka onward, concentrations of the sea ice, open ocean, and terrestrial biomarkers all increase simultaneously. IP_{25} peaks early in T II, while brassicasterol, dinosterol, campesterol, and sitosterol peak later in the same period. Toward the end of T II, all the biomarker concentrations decrease simultaneously. At this stage, IP_{25} concentrations become undetectable, while the concentrations of brassicasterol, dinosterol, sitosterol, and campesterol remain very low. During MIS 5e and the remainder of MIS 5d–b, IP_{25} is not detected again, whereas the open ocean and terrestrial biomarkers persist at very low concentrations.

5. Discussion

5.1. MIS 6 (pre-T II) extensive sea ice cover and polynyas

During late MIS 6 (pre-T II) (140–135 ka), an extensive sea ice cover likely prevailed in the eastern Fram Strait, consistent with low Northern Hemisphere summer insolation (Fig. 5A). The low biomarker concentrations at KH-14 suggest that the extensive sea ice cover limited the light and nutrient availability, inhibiting the growth of ice algae and open-water phytoplankton (cf. Müller et al., 2011). However, occasional increases in IP_{25} (Fig. 4B), brassicasterol and dinosterol (Fig. 4C) indicate intermittent seasonally ice-free periods. The presence of planktic foraminifers at KH-14, along with similar findings at ODP Site 986 (Zhuravleva et al., 2017), further supports seasonally open waters along the western Svalbard margin (Hebbeln and Wefer, 1997; Spielhagen et al., 2004).

Several biomarker records from the Fram Strait provide evidence of occasional seasonal variability during late MIS 6 (pre-T II) (Fig. 5D–H). Studies by Stein et al. (2017) and Kremer et al. (2018a, 2018b) reported occurrences of IP_{25}, phytoplankton, and terrigenous biomarkers along the Barents Sea margin, the Yermak Plateau, and in the eastern Fram Strait, indicating intermittent open-water conditions. The occasional presence of seasonally open water conditions in the otherwise perennially sea ice-covered Fram Strait and Yermak Plateau argues against the hypothesis of an extensive ice shelf extending from the central Arctic Ocean as some studies have proposed (Jakobsson et al., 2016; Geibert et al., 2021). Instead, these findings support the concept of a perennial sea ice-covered Arctic Ocean during late MIS 6, as proposed by Stein et al. (2017, 2022).

Katabatic winds, created when the SBIS likely extended onto the continental margin (Svendsen et al., 2004), along with upwelling of warm Atlantic waters, likely led to the formation of coastal polynyas along the western and northern Svalbard margin (Fig. 6) (e.g., Knies and Stein, 1998; Matthiessen and Knies, 2001; Stein et al., 2017). These winds pushed sea ice away from the shelf edge, creating open waters where melting ice released nutrients and sediments, increasing the fluxes of ice algae, open-water phytoplankton, and terrigenous matter. At KH-14, slightly elevated IP_{25} concentrations (Fig. 4B) suggest small, occasional polynyas in the eastern Fram Strait. Farther north, higher IP_{25} concentrations in cores PS2138 (Fig. 5H; Stein et al., 2017), and PS92/039 (Fig. 5G; Kremer et al., 2018b), indicate more extensive polynya activity. These meridional differences suggest stronger katabatic winds and/or greater ice sheet extent farther north, resulting in more extensive sea ice farther to the south in the Fram Strait. Additionally, variability in nutrient availability and biomarker flux may reflect differences in polynya dynamics. The northernmost sites may have experienced repeated polynya openings and closures, releasing more nutrients from sea ice and enhancing productivity. In contrast, a single annual polynya opening at the southernmost site may have resulted in smaller nutrient inputs and lower overall productivity.

Warm Atlantic waters likely played an additional important role in late MIS 6 (pre-T II) sea ice conditions, similar to its role today in the Fram Strait (e.g., Walczowski and Piechura, 2011; Polyakov et al., 2017). The increased magnetic susceptibility in our late MIS 6 record could suggest enhanced influence of Atlantic waters (Fig. 4G). Risebrobakken et al. (2006) linked higher magnetic susceptibility in core MD99-2303 to a strengthened northern extension of the surface branch of the Atlantic Meridional Overturning Circulation (AMOC), similar to MIS 3 (Kissel et al., 1999). These authors proposed that magnetic material likely originated from the Iceland-Faroe-Shetland and the Knipovich Ridge systems (Fig. 1), the latter being a mid-oceanic ridge system that directs the northward flowing branch of the deep water. They also noted a consistent presence of chalk fragments in a transect from the Nordic Seas to the Fram Strait, providing additional evidence for active northward surface transport by chalk-carrying icebergs. Combined with the increased magnetic susceptibility, their evidence suggests periods with active northward transport of Atlantic waters. Several studies have indicated a reduced, yet sustained, influence of Atlantic waters during MIS 6 and other glacial periods (Henrich, 1998; Knies et al., 1999; Ezat et al., 2014; Zhuravleva et al., 2017). Nørgaard-Pedersen et al. (2003) proposed that, during the Last Glacial Maximum, Atlantic waters may have shallowed due to reduced halocline thickness, or due to a relative strengthening of the Fram Strait branch at the expense of a blocked Barents Sea branch. A similar configuration of Atlantic waters during late MIS 6 would likely have contributed to the occasional break-up of sea ice in the Fram Strait and along the Svalbard-Barents Sea margin.

5.2. Termination II: From perennial to marginal sea ice

At the onset of T II (ca. 135 ka), perennial sea ice likely formed during a short time interval in the eastern Fram Strait, suggested by the decline of IP_{25} and the open-water phytoplankton biomarkers, along with a PIP_{25} index of 1 (Fig. 5E). Supporting this interpretation are the low Ca/Ti ratios, TOC %, IRD counts (Fig. 4E–H) and terrigenous biomarker concentrations (Fig. 4D), all suggesting a minimal vertical flux of sediment and biogenic material under extensive sea ice. Alternatively, oligotrophic conditions caused by massive meltwater discharges may have reduced surface-water productivity and, consequently, the biomarker concentrations (cf. You et al., 2023). This alternative interpretation is further supported by the decrease in planktic $\delta^{18}O$ at 135 ka (Fig. 2A), indicating dilution of surface waters by ^{18}O-depleted meltwater.

The early T II episode with perennial sea ice and/or meltwater discharge was brief, lasting about 2000 years. From ca. 133 ka, profound oceanographic changes occurred. High concentrations of IP_{25}, dinosterol, brassicasterol, campesterol and sitosterol (Fig. 4B–D) indicate favourable conditions for sea ice and open water algal growth, accompanied by a continuous input of terrigenous material. Such conditions have previously been reported as typical features along the marginal ice zone (Stein et al., 2016). P_BIP_{25} and P_DIP_{25} values between 0.50 and 0.75 (Fig. 5E) further support this (cf. Müller et al., 2011), as do the presence of RBCs and *I. minutum* (Fig. 5C) indicating a highly productive environment with seasonal sea ice (Marret et al., 2004; de Vernal et al., 2020b). Along with increased Northern Hemisphere summer insolation (Fig. 5A), enhanced sea ice melt subsequently led to the establishment of a marginal ice zone at site KH-14 (Fig. 6).

The high biomarker concentrations observed during T II were likely also determined by sedimentary processes related to the retreating SBIS. Elevated TOC at site KH-14 (Fig. 4E) suggests enhanced organic matter preservation and/or surface productivity (e.g., Emerson and Hedges,

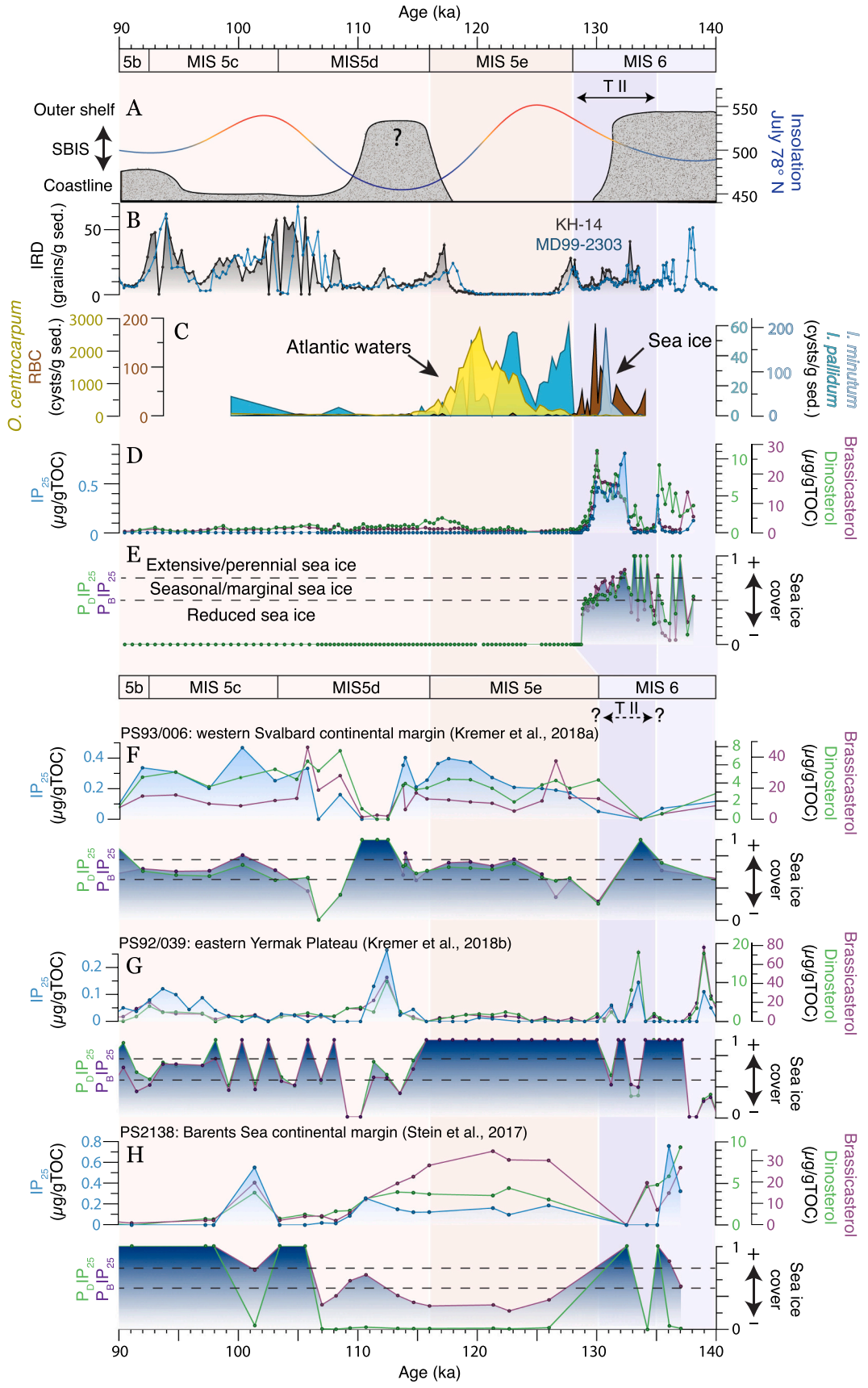

(caption on next page)

Fig. 5. A) Mean July Northern Hemisphere insolation at 78° N (Laskar et al., 2004) and extent of the Svalbard–Barents Sea Ice Sheet (SBIS) on the continental shelf (Svendsen et al., 2004), B) IRD from cores KH-14 and MD99-2303 (Risebrobakken et al., 2005, 2006), C) concentrations of four selected dinocyst species discussed in the text; *O. centrocarpum* (Atlantic waters), *I. pallidum* (cool water), *I. minutum* and RBCs (cool waters and sea ice), D) concentrations of IP_{25} (sea ice), brassicasterol and dinosterol (open ocean), E) P_BIP_{25} (B-brassicasterol) and P_DIP_{25} (D-dinosterol) indexes representing sea ice cover from perennial (1) to open ocean (0). Sea ice interpretations following Müller et al. (2011) are marked with dashed lines; values 0.75–1.00 refer to a permanent sea ice cover throughout the year, 0.50–0.75 reflect seasonal ice cover or a stable ice edge, and 0.00–0.50 indicate less ice or ice-free conditions, F) biomarker concentration and PIP_{25} indexes from core PS93/006 (Kremer et al., 2018a) (see D and E for details), G) biomarker concentration and PIP_{25} indexes from core PS92/039 (Kremer et al., 2018b) (see D and E for details), H) biomarker concentrations and PIP_{25} indexes from core PS2138 (Stein et al., 2017) (see D and E for details).

1988; Canfield, 1994). Simultaneous high concentrations of marine, sea ice, and terrestrial biomarkers, along with high TOC, have been linked to deglacial phases when the retreating SBIS released continuous turbid meltwater and high amounts of suspended fine-grained terrestrial organic matter (Knies and Stein, 1998; Kremer et al., 2018b; Köseoğlu et al., 2019). This deglacial influx may have boosted primary productivity and accelerated the vertical transfer of marine organic matter to the seafloor by forming large aggregates of marine and terrigenous particles (Knies and Stein, 1998). Additionally, the formation of new sea ice at the marginal ice zone may have entrapped terrigenous material which, when released later in the melt season, would increase the nutrient supply in the euphotic zone and elevate surface water productivity (Nelson et al., 1989; Fahl and Stein, 1997; Sakshaug, 2004).

The ocean biological pump likely increased during T II due to several factors related to changes in sea ice conditions. As the Fram Strait transitioned from perennial to marginal sea ice, vast areas of CO_2-undersaturated waters may have been exposed, enhancing CO_2 uptake into the surface ocean (Bates et al., 2006). Additionally, brine formation during annual sea ice regrowth in the marginal ice zone facilitated the entrainment of surface waters to the deep ocean. These processes, combined with increased primary productivity and rapid vertical transport of phytoplankton organic matter, created conditions that influenced water column alkalinity and pH which may have impacted the preservation of biogenic carbonate remains on the seafloor (Steinsund and Hald, 1994; Knies et al., 1999; de Vernal et al., 2020a). Indeed, the decrease of Ca/Ti and the almost complete absence of benthic and planktic foraminifers at KH-14 (132–128 ka), suggest extensive carbonate dissolution during part of T II. While dilution of biotic components or lowered productivity (Ruddiman et al., 1980) may also explain the foraminiferal-barren intervals, this would require a marked increase in sedimentation rates, which only increased modestly from 8 cm/ka during MIS 6 to 9 cm/ka in T II. Moreover, elevated sea ice and open-water biomarker concentrations imply relatively increased productivity rather than terrestrial biogenic input, suggesting dissolution at the sea floor as the plausible explanation. Similar patterns of low XRF-Ca and foraminifer-barren intervals were observed at sites MD99-2303 and ODP986 during T II (Risebrobakken et al., 2006; Zhuravleva et al., 2017). Additionally, periods with enhanced organic carbon and low to zero carbonate contents have been observed along the northern Eurasian margin of the Arctic Ocean during the late Quaternary and have been associated with movements of the SBIS (Elverhøi et al., 1995; Knies and Stein, 1998; Stein et al., 2001; Vogt et al., 2001; Winkelmann et al., 2008; Kremer et al., 2018b). Thus, we postulate that a coupling of sedimentary processes linked to SBIS retreat, a high-productivity sea ice environment, and newly exposed CO_2-undersaturated open waters at the marginal ice zone, played a vital role in shaping an environment that enhanced the biological pump during T II.

The SBIS retreat during T II likely also caused a substantial influx of meltwater, as indicated by a major decrease in *N. pachyderma* $\delta^{18}O$ (Fig. 2A). IRD (Fig. 4G) and coal fragments (606–615 cm; Supplementary Fig. 1) at KH-14, in line with observations from ODP Site 986 and MD99-2303 (Zhuravleva et al., 2017; Risebrobakken et al., 2006), further suggest the SBIS as a possible source. This meltwater input may have impeded the northward expansion of Atlantic waters (Bauch et al., 1999), as indicated by low magnetic susceptibility at KH-14 (Fig. 4G), possibly implying a weakening of the Atlantic waters inflow (cf. Risebrobakken et al., 2006). Alternatively, the meltwater input likely reinforced a strong halocline, suppressing northward-flowing Atlantic waters to the subsurface (Zhuravleva et al., 2017), stabilising the marginal ice zone by reducing the upward heat flux of Atlantic waters. The latter interpretation is supported by enhanced sea ice cover farther north in the Fram Strait, with perennial sea ice at site PS2138 (Fig. 5H; Stein et al., 2017) and seasonal to extensive sea ice at sites PS93/006 (Fig. 5F; Kremer et al., 2018a) and PS92/039 (Fig. 5G; Kremer et al., 2018b). However, we must point out that while the environmental reconstructions from these sites are broadly contemporaneous, they may not align exactly. Comparing palaeoceanographic records across the Fram Strait and into the Arctic Ocean is challenging due to the generally low temporal resolution and age model uncertainties at each site, often due to the lack of isotopic data, and further compounded by local climatic and/or oceanographic overprints.

5.3. MIS 5e: An open ocean and intensification of Atlantic waters influence

Shortly before the onset of MIS 5e (128 ka), low to absent concentrations of sea ice and open-water phytoplankton biomarkers indicate either open waters or perennial sea ice in the eastern Fram Strait (Fig. 6). Nevertheless, other evidence favours open-water dominance. For example, the concentration of IRD is low from 128 ka and nearly zero from 126 to 120 ka (Fig. 5b), indicating a lack of sea ice and icebergs necessary for IRD transport (e.g. Stein et al., 2012). In early MIS 5e (128–124 ka) the presence of *I. pallidum* (Fig. 3; 5C) indicates a cool, open-ocean environment, as this species is today typically found in the cold, open ocean of the Arctic water domain between the EGC and WSC (Marret and Zonneveld, 2003). Farther north, on the Barents Sea margin (PS2138), progressively cooler surface ocean conditions are reflected by the presence of sea ice-related dinocysts *I. minutum* and RBCs in the earliest MIS 5e (Assemblage Zone 1 of Matthiessen and Knies (2001)). This indicates extensive seasonal sea ice and increased surface water production there, corroborated by IP_{25} findings at the same site (Stein et al., 2017).

The cool open ocean conditions in early MIS 5e suggest a "delayed" onset of "warm" optimum climatic conditions in the eastern Fram Strait, similar to results of Risebrobakken et al. (2011) for the Early Holocene when insolation forcing dominated surface ocean changes. The "delayed" warming likely resulted from the continued existence of a cold and fresh surface layer following the long deglaciation (e.g., Rasmussen et al., 2003b; Thibodeau et al., 2017; Bauch, 2013), which would have prevented subsurface Atlantic waters from mixing with the surface ocean. Indeed, several studies from the Nordic Seas have demonstrated that deglacial processes continued well into the low $\delta^{18}O$ interval of MIS 5e, suggesting substantial meltwater discharge and cold regional conditions in early MIS 5e (e.g., Baumann et al., 1995; Bauch et al., 1996; Kellogg et al., 1978; Haake and Pflaumann, 1989; Fronval and Jansen, 1997; Bauch et al., 2000; Rasmussen et al., 2003b).

Interglacial optimal "warm" conditions during MIS 5e started ca. 4500 years after the interglacial onset, as indicated by the increasing concentrations of *O. centrocarpum* (Fig. 5C) and the presence *S. mirabilis* (Fig. 3), both associated with interglacial optima in the northern North Atlantic (Sánchez Goñi et al., 1999; Eynaud et al., 2004; Penaud et al., 2008; Van Nieuwenhove et al., 2008, 2011). High *O. centrocarpum* concentrations and *S. mirabilis* presence suggest conditions favourable for dinoflagellate production. Thus, a sea ice margin was likely located

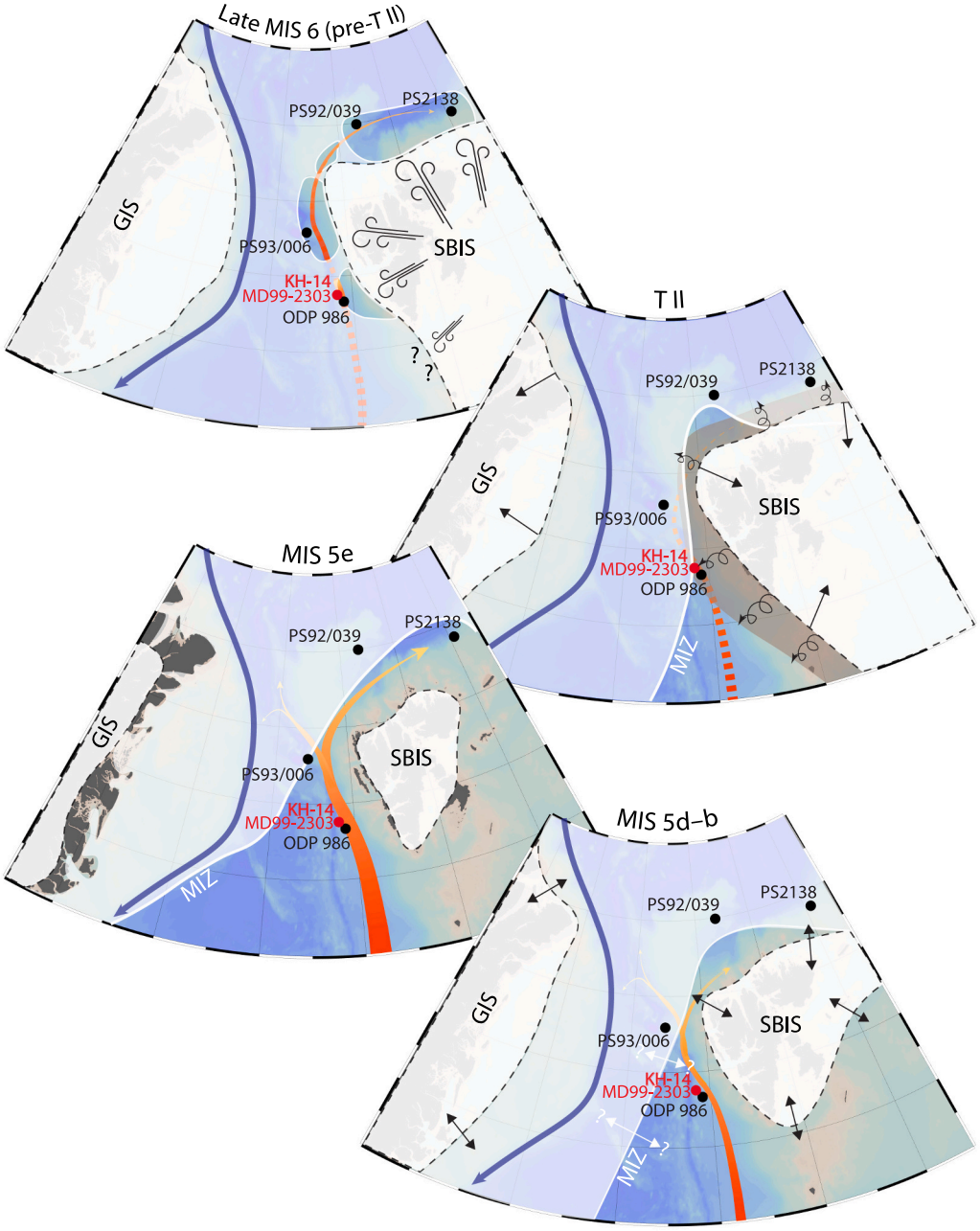

Fig. 6. Schematic illustration of sea ice conditions in the Fram Strait during late MIS 6 (pre-T II), T II, MIS 5e, and MIS 5d–b, summarising the data presented in Fig. 5. The schematic illustrates sea ice cover (white shaded area), and its extent marked by the marginal ice zone (MIZ). Tentative extents of the Greenland Ice Sheet (GIS) and the Svalbard–Barents Sea Ice Sheet (SBIS) are based on the reconstructions by Batchelor et al. (2019) and Vasskog et al. (2015) with associated arrows indicating their general retreats or advances. The influence of Atlantic waters via the West Spitsbergen Current (WSC) is indicated with orange lines, showing surface influence (solid lines) and subsurface influence (dashed lines). Late MIS 6: An extensive sea ice cover was periodically interrupted by local polynyas formed due to strong katabatic winds and intrusions of Atlantic waters. T II: A marginal ice zone developed, and the environment was influenced by the influx of organic-matter-rich meltwater suspended from the retreating SBIS (brown shaded area with arrows along the Svalbard margin), with limited influence of subsurface Atlantic waters on the sea ice cover. MIS 5e: Predominantly sea ice-free conditions prevailed, and Atlantic waters dominated the surface ocean. MIS 5d–b: Sea ice conditions remain ambiguous, and the influence of Atlantic waters on the surface ocean was small, yet persistent. (For interpretation of the references to colour in this figure legend, the reader is referred to the web version of this article.)

farther north than site KH-14, and the surface ocean was substantially influenced by Atlantic waters, peaking at ca. 120 ka. At this time, when *O. centrocarpum* reached maximum concentrations, we also recorded high Ca/Ti (Fig. 4F; 5C), and consistent presence of benthic and planktic foraminifers. Additionally, at MD99-2303 (Risebrobakken et al., 2006), planktic and benthic foraminifers reappear at ca. 122.5 ka (Fig. 2A), and at ODP 986, Zhuravleva et al. (2017) note substantially improved preservation of carbonate foraminiferal shells. Good carbonate preservation and high Ca were associated with increased influence of Atlantic waters in Early Holocene sediments (Rasmussen et al., 2007; Zamelczyk et al., 2014; Werner et al., 2016) and may similarly reflect the phase with the strongest influence of Atlantic waters in the eastern Fram Strait during MIS 5e (Zhuravleva et al., 2017).

The warmest optimal interglacial conditions thus likely occurred in

late MIS 5e, consistent with previous studies in the region (e.g., Bauch et al., 1999; Risebrobakken et al., 2005, 2007; Van Nieuwenhove et al., 2011; Zhuravleva et al., 2017). However, it also contrasts with studies suggesting peak interglacial warmth in the earliest MIS 5e, particularly from coring sites located in the central Nordic Seas (e.g., Bauch et al., 2012; Bauch, 2013), along the Faroe-Shetland Channel (Rasmussen et al., 2003b), south of the Iceland-Scotland Ridge (Eynaud et al., 2004; Penaud et al., 2008), and the Labrador Sea (Rasmussen et al., 2003a; Irvali et al., 2012, Irvali et al., 2016; Steinsland et al., 2023). This discrepancy suggests that the locus of Atlantic water transport and related heat may have varied between the Nordic Seas and the North Atlantic (e.g. Bauch et al., 1999). One explanation is that a contracted subpolar gyre in late MIS 5e led to a relative increase of inflowing Atlantic waters to the Nordic Seas and Fram Strait while reducing its westward flow across the North Atlantic (Born et al., 2011). In contrast, an expanded subpolar gyre in early MIS 5e may have directed relatively more Atlantic waters westward in the North Atlantic, delaying warming in the Fram Strait. This pattern aligns with evidence of early warming in the western North Atlantic (Rasmussen et al., 2003b; Eynaud et al., 2004; Penaud et al., 2008; Irvali et al., 2012; Irvali et al., 2016; Mokeddem et al., 2014; Steinsland et al., 2023). Thus, the spatial pattern of climate evolution through the interglacial may be most easily understood as a consequence of the evolving pattern of large-scale surface circulation and associated heat transports.

A second explanation proposed for the late increased presence of warm Atlantic waters at the surface is a shift to a more positive North Atlantic Oscillation (NAO) mode (Bauch and Kandiano, 2007; Risebrobakken et al., 2007). This was similarly suggested as a mechanism responsible for the peak sea surface temperatures in the North Atlantic during the Early Holocene (Rimbu et al., 2003). Modern observations support this as Blindheim et al. (2000) found that a positive NAO narrows the Norwegian Atlantic Current, reducing cooling by limiting the surface area Atlantic waters exposed to the atmosphere, thereby extending heat transport northward.

Thirdly, Zhuravleva et al. (2017) suggest that coring sites in the central Nordic Seas, being farther from the collapsing European and Greenland ice sheets, were less influenced by deglacial freshwater, implying that the early cool signal along the Norwegian-Svalbard margin was likely due to a thick halocline from post-deglaciation meltwater input rather than, for example, a reduced influx of Atlantic waters to the Fram Strait. Regardless of the mechanisms that controlled the influence and/or influx of Atlantic waters in the Fram Strait, it is clear that Atlantic waters profoundly influenced the sea ice cover throughout MIS 5e. Cores near the main flow path of Atlantic waters (PS2138 and KH-14) show reduced sea ice cover, while regions in Arctic waters (PS93/0061 and PS92/039) experienced extensive (PS93/0061) to perennial sea ice (PS92/039) (Figs. 5–6). Such contrasting conditions between cores of relatively short distances suggest a very sharp sea ice gradient in the surface ocean during MIS 5e, similar to sea ice conditions in the modern Fram Strait (Fig. 1).

5.4. MIS 5d–b: Surface cooling and unresolved sea ice proxy signals

As summer insolation decreased (Fig. 5A), surface ocean cooling marked the transition into MIS 5d as illustrated by the increased relative abundance of *N. labyrinthus* (Fig. 3). This subpolar to temperate species thrives where Atlantic waters mix with cold Arctic waters (Rochon et al., 1999; Marret et al., 2004). Its high abundances in the North Atlantic, Nordic Seas, and Fram Strait align with the MIS 5e–5d transition in polar to subpolar regions influenced by Atlantic waters (Matthiessen and Knies, 2001; Eynaud et al., 2004; Van Nieuwenhove et al., 2008, 2011).

Despite cooler surface ocean conditions during MIS 5d, it remains unclear whether there was sea ice at site KH-14. Similar to MIS 5e, the absence of IP_{25} coupled with low concentrations of open-water phytoplankton biomarkers suggest either open ocean or perennial sea ice conditions. The sustained and variable influx of IRD, coal, and TOC around 106 and 94 ka (Fig. 4E, F, H) likely indicate major ice sheet advances consistent with observations on the western continental margin of Svalbard (Mangerud et al., 1996, 1998), and the Siberia and the Kara Sea during MIS 5d–b (Svendsen et al., 2004). This also coincides with an extended sea ice cover at the northern Barents Sea continental margin (Stein et al., 2017). Despite large environmental changes, the lack of variability in IP_{25} raises the possibility of poor biomarker preservation during MIS 5d–b at our site. One explanation may have been a low surface ocean productivity. If the production of phytoplankton and ice algae is low (if any) at the surface ocean, additional processes like zooplankton grazing, transport through the water column, and degradation at the seafloor and in the sediment can make it hard for the original algae concentrations to preserve. Additionally, the naturally lower production of IP_{25} relative to brassicasterol and dinosterol in the surface ocean could explain why our record contains zero IP_{25} and still a low but persistent presence of the open ocean biomarkers (Fig. 4B–D). Another explanation for the absence of IP_{25} may have been that environmental conditions were not suitable for its production. It was reported that individual *Haslea* spp., the diatoms responsible for IP_{25} production, obtained from Canadian Arctic samples yielded $C_{25:3}$ and $C_{25:4}$ HBIs, but not IP_{25} (Belt and Müller, 2013). This suggests that IP_{25} production may require specific sea ice conditions (e.g. Belt and Müller, 2013; Limoges et al., 2018b). Thus, in some sea ice environments we do not find IP_{25} in the sediment, although in most cases we do.

In summary, our MIS 5d–b biomarkers are inconclusive regarding sea ice conditions. While low dinocyst concentrations suggest reduced surface productivity and oligotrophic conditions, the absence of typical sea ice species like RBCs or *I. minutum* (Fig. 3) imply that the surface ocean may have been ice-free, at least seasonally. The persistent presence of *O. centrocarpum*, albeit at lower concentrations, indicates continued but diminished influence of Atlantic waters, potentially facilitating the regrowth of perennial sea ice farther north, as observed at site PS2138 on the Barents Sea continental margin (Fig. 5H; Stein et al., 2017). The shift to a low-productivity environment may have been caused by an eastward and southward expansion of Arctic water in the Fram Strait, similarly suggested for other events of cooling in the eastern Fram Strait (Hebbeln and Wefer, 1997; Rasmussen et al., 2003b; Risebrobakken et al., 2007). However, further research is needed to clarify the sea ice conditions during this period, particularly given the unexpected biomarker signals. If the Fram Strait was ice-free during MIS 5d–b it suggests that cooler conditions than those at the onset of the Weichselian glaciation, when northern hemisphere summer insolation values were similar to modern, were necessary for sea ice to return.

6. Conclusions

Our high-resolution, multiproxy record from late MIS 6 to MIS 5e–b provides detailed insights into sea ice cover, Atlantic water influence, and ice sheet dynamics in the eastern Fram Strait. During late MIS 6 (pre-T II), extensive sea ice was intermittently disrupted by seasonal melt, likely driven by local polynyas formed from katabatic winds and Atlantic water intrusions. During T II, sea ice transitioned from perennial to a productive marginal ice zone. The marginal ice zone environment, combined with organic matter-rich meltwater influx from the SBIS, may have increased the biological pump in the eastern Fram Strait. The meltwater likely maintained a thick halocline, limiting the influence of subsurface Atlantic waters on the sea ice cover. By MIS 5e, the region was likely sea ice-free and dominated by Atlantic waters, with peak warming and the strongest influence around 120 ka. Throughout MIS 5d–b, the SBIS shaped the sedimentary environment, with dinocysts suggesting oligotrophic conditions and an eastward expansion of Arctic waters. However, unusual biomarker concentrations complicate definitive conclusions on sea ice conditions during this period, highlighting the need for further research to clarify environmental conditions at the onset of the Weichselian glaciation.

CRediT authorship contribution statement

Kristine Steinsland: Writing – review & editing, Writing – original draft, Project administration, Methodology, Investigation, Conceptualization. **Danielle M. Grant:** Writing – review & editing. **Kirsten Fahl:** Writing – review & editing, Supervision, Methodology, Data curation. **Ruediger Stein:** Writing – review & editing, Methodology, Supervision, Data curation. **Tine L. Rasmussen:** Writing – review & editing, Methodology, Data curation. **Bjørg Risebrobakken:** Writing – review & editing, Methodology. **Ulysses S. Ninnemann:** Writing – review & editing, Methodology, Supervision, Data curation. **Jochen Knies:** Writing – review & editing. **Julie Heggdal Velle:** Writing – review & editing. **Stijn De Schepper:** Writing – review & editing, Writing – original draft, Supervision, Methodology, Conceptualization.

Declaration of competing interest

The authors declare that they have no known competing financial interests or personal relationships that could have appeared to influence the work reported in this paper.

Acknowledgements

We thank the researchers and crew of the CAGE19-3 cruise with RV Kronprins Haakon. We thank Walter Luttmer in the biomarker laboratory, Dag Inge Blindheim for technical support, Malcolm Jones at Palynological Laboratory Service Ltd. for the preparation of the palynological slides, and Eivind Støren for the help with core scanning (Earthlab, University of Bergen). XRF logging data from MD99-2303 were generated by Thomas Richter while employed at the Royal Netherlands Institute of Sea Research and are kindly provided for this study. We are grateful to Catherine Kissel for helpful discussions on the manuscript and methodology of core MD99-2303. This study is part of the AGENSI project, which has received funding from the European Research Council (ERC) under the European Union's Horizon 2020 research and innovation program (grant agreement No 818449). The research received support from the ERC Synergy project i2B, grant number 101118519. BR acknowledges funding from the Research Council of Norway (project 325333). TLR and JK were supported by the Research Council of Norway through its Centers of Excellence funding scheme, project number 223259.

Appendix A. Supplementary data

Supplementary data to this article can be found online at https://doi.org/10.1016/j.palaeo.2025.112779.

Data availability

All data is available on PANGAEA, https://doi.org/10.1594/PANGAEA.973596 (Steinsland et al., 2025).

References

Aagaard, K., 1982. Inflow from the Atlantic Ocean to the Polar Basin. In: Rey, L. (Ed.), The Arctic Ocean: The Hydrographic Environment and the Fate of Pollutants. Palgrave Macmillan UK, London, pp. 69–81. https://doi.org/10.1007/978-1-349-05919-5_3.

Aagaard, K., Coachman, L.K., 1968. The East Greenland Current North of Denmark Strait: part I. Arctic 21, 181–200. https://doi.org/10.14430/arctic3262.

Allen, M.R., de Coninck, H., Dube, O.P., Hoegh-Guldberg, O., Jacob, D., Jiang, K., Revi, A., Rogelj, J., Roy, J., Shindell, D., Solecki, W., Taylor, M., Tschakert, P., Waisman, H., Abdul Halim, S., Antwi-Agyei, P., Aragón-Durand, F., Babiker, M., Bertoldi, P., Bindi, M., Brown, S., Buckeridge, M., Camilloni, I., Cartwright, A., Cramer, W., Dasgupta, P., Diedhiou, A., Djalante, R., Dong, W., Ebi, K.L., Engelbrecht, F., Fifita, S., Ford, J., Forster, P., Fuss, S., Ginzburg, V., Guiot, J., Handa, C., Hayward, B., Hijioka, Y., Hourcade, J.-C., Humphreys, S., Kainuma, M., Kala, J., Kanninen, M., Kheshgi, H., Kobayashi, S., Kriegler, E., Ley, D., Liverman, D., Mahowald, N., Mechler, R., Mehrotra, S., Mulugetta, Y., Mundaca, L., Newman, P., Okereke, C., Payne, A., Perez, R., Pinho, P.F., Revokatova, A., Riahi, K., Schultz, S., Séférian, R., Seneviratne, S.I., Steg, L., Suarez Rodriguez, A.G., Sugiyama, T., Thomas, A., Vilariño, M.V., Wairiu, M., Warren, R., Zickfeld, K., Zhou, G., 2018. In: Masson-Delmotte, V., Zhai, P., Pörtner, H.-O., Roberts, D., Skea, J., Shukla, P.R., Pirani, A., Moufouma-Okia, W., Péan, C., Pidcock, R., Connors, S., Matthews, J.B.R., Chen, Y., Zhou, X., Gomis, M.I., Lonnoy, E., Maycock, T., Tignor, M., Waterfield, T. (Eds.), Technical Summary. In: Global Warming of 1.5°C. An IPCC special Report on the impacts of global warming of 1.5°C above pre-industrial levels and related global greenhouse gas emission pathways, in the context of strengthening the global response to the threat of climate change, sustainable development, and efforts to eradicate poverty. Cambridge University Press, Cambridge, UK and New York, NY, USA, pp. 27–46. https://doi.org/10.1017/9781009157940.002.

Batchelor, C.L., Margold, M., Krapp, M., Murton, D.K., Dalton, A.S., Gibbard, P.L., Stokes, C., Murton, R.J.B., Manica, A., 2019. The configuration of Northern Hemisphere ice sheets through the Quaternary. Nat. Commun. 10, 3713. https://doi.org/10.1038/s41467-019-11601-2.

Bates, N.R., Moran, S.B., Hansell, D.A., Mathis, J.T., 2006. An increasing CO_2 sink in the Arctic Ocean due to sea-ice loss. Geophys. Res. Lett. 33. https://doi.org/10.1029/2006GL027028.

Bauch, H.A., 2013. Interglacial climates and the Atlantic meridional overturning circulation: is there an Arctic controversy? Quat. Sci. Rev. 63, 1–22. https://doi.org/10.1016/j.quascirev.2012.11.023.

Bauch, H.A., Kandiano, E., 2007. Evidence for early warming and cooling in North Atlantic surface waters during the last interglacial. Paleoceanography 22. https://doi.org/10.1029/2005PA001252.

Bauch, H.A., Erlenkeuser, H., Grootes, P.M., Jouzel, J., 1996. Implications of Stratigraphic and Paleoclimatic Records of the Last Interglaciation from the Nordic Seas. Quat. Res. 46, 260–269. https://doi.org/10.1006/qres.1996.0065.

Bauch, H.A., Erlenkeuser, H., Fahl, K., Spielhagen, R.F., Weinelt, M.S., Andruleit, H., Henrich, R., 1999. Evidence for a steeper Eemian than Holocene Sea surface temperature gradient between Arctic and sub-Arctic regions. Palaeogeogr. Palaeoclimatol. Palaeoecol. 145, 95–117. https://doi.org/10.1016/S0031-0182(98)00104-7.

Bauch, H.A., Erlenkeuser, H., Jung, S.J.A., Thiede, J., 2000. Surface and deep water changes in the subpolar North Atlantic during termination II and the last Interglaciation. Paleoceanography 15, 76–84. https://doi.org/10.1029/1998PA000343.

Bauch, H.A., Kandiano, E.S., Helmke, J.P., 2012. Contrasting Ocean changes between the subpolar and polar North Atlantic during the past 135 ka. Geophys. Res. Lett. 39. https://doi.org/10.1029/2012GL051800.

Baumann, K.-H., Lackschewitz, K.S., Mangerud, J., Spielhagen, R.F., Wolf-welling, T.C. W., Henrich, R., Kassens, H., 1995. Reflection of Scandinavian Ice Sheet Fluctuations in Norwegian Sea Sediments during the past 150,000 years. Quat. Res. 43, 185–197. https://doi.org/10.1006/qres.1995.1019.

Belt, S.T., 2018. Source-specific biomarkers as proxies for Arctic and Antarctic Sea ice. Org. Geochem. 125, 277–298. https://doi.org/10.1016/j.orggeochem.2018.10.002.

Belt, S.T., Müller, J., 2013. The Arctic Sea ice biomarker IP_{25}: a review of current understanding, recommendations for future research and applications in palaeo sea ice reconstructions. Quat. Sci. Rev. 79, 9–25. https://doi.org/10.1016/j.quascirev.2012.12.001.

Belt, S.T., Massé, G., Rowland, S.J., Poulin, M., Michel, C., LeBlanc, B., 2007. A novel chemical fossil of palaeo sea ice: IP25. Org. Geochem. 38, 16–27. https://doi.org/10.1016/j.orggeochem.2006.09.013.

Blindheim, J., Borovkov, V., Hansen, B., Malmberg, S.AA., Turrell, W.R., Østerhus, S, 2000. Upper layer cooling and freshening in the Norwegian Sea in relation to atmospheric forcing. Deep Sea Res. Part Oceanogr. Res. Pap. 47, 655–680. https://doi.org/10.1016/S0967-0637(99)00070-9.

Boon, J.J., Rijpstra, W.I.C., De Lange, F., De Leeuw, J.W., Yoshioka, M., Shimizu, Y., 1979. Black Sea sterol—a molecular fossil for dinoflagellate blooms. Nature 277, 125–127. https://doi.org/10.1038/277125a0.

Born, A., Nisancioglu, K.H., Risebrobakken, B., 2011. Late Eemian warming in the Nordic Seas as seen in proxy data and climate models. Paleoceanography 26. https://doi.org/10.1029/2010PA002027.

Bourke, R.H., Weigel, A.M., Paquette, R.G., 1988. The westward turning branch of the West Spitsbergen current. J. Geophys. Res. Oceans 93, 14065–14077. https://doi.org/10.1029/JC093iC11p14065.

Broecker, W.S., 1997. Thermohaline Circulation, the Achilles Heel of our climate System: will Man-made CO_2 upset the Current Balance? Science 278, 1582–1588.

Brown, T.A., Belt, S.T., Tatarek, A., Mundy, C.J., 2014. Source identification of the Arctic Sea ice proxy IP_{25}. Nat. Commun. 5, 4197. https://doi.org/10.1038/ncomms5197.

Canfield, D.E., 1994. Factors influencing organic carbon preservation in marine sediments. Chem. Geol. 114, 315–329. https://doi.org/10.1016/0009-2541(94)90061-2.

De Schepper, S., Beck, K.M., Mangerud, G., 2017. Late Neogene Dinoflagellate Cyst and Acritarch Biostratigraphy for Ocean Drilling Program Hole 642B, Norwegian Sea. Rev. Palaeobot. Palynol. https://doi.org/10.1016/j.revpalbo.2016.08.005.

de Vernal, A., Gersonde, R., Goosse, H., Seidenkrantz, M.-S., Wolff, E.W., 2013. Sea ice in the paleoclimate system: the challenge of reconstructing sea ice from proxies – an introduction. Quat. Sci. Rev. Sea Ice in the Paleoclimate System: the Challenge of Reconstructing Sea Ice from Proxies 79, 1–8. https://doi.org/10.1016/j.quascirev.2013.08.009.

de Vernal, A., Hillaire-Marcel, C., Le Duc, C., Roberge, P., Brice, C., Matthiessen, J., Spielhagen, R.F., Stein, R., 2020a. Natural variability of the Arctic Ocean sea ice during the present interglacial. Proc. Natl. Acad. Sci. 117, 26069–26075. https://doi.org/10.1073/pnas.2008996117.

de Vernal, A., Radi, T., Zaragosi, S., Van Nieuwenhove, N., Rochon, A., Allan, E., De Schepper, S., Eynaud, F., Head, M.J., Limoges, A., Londeix, L., Marret, F., Matthiessen, J., Penaud, A., Pospelova, V., Price, A., Richerol, T., 2020b. Distribution of common modern dinoflagellate cyst taxa in surface sediments of the Northern Hemisphere in relation to environmental parameters: the new n=1968 database. Mar. Micropaleontol., Taxonomy and distribution of modern organic-walled dinoflagellate cysts in surface sediments from the Northern Hemisphere: an update of Rochon et al, 159, p. 101796. https://doi.org/10.1016/j.marmicro.2019.101796.

Dieckmann, G.S., Hellmer, H.H., 2008. The Importance of Sea Ice: An Overview. In: Thomas, D.N., Diekmann, G.S. (Eds.), Sea Ice: An Introduction to its Physics, Chemistry, Biology, and Geology. Blackwell Science, Oxford, pp. 1–21.

Elverhøi, A., Svendsen, J.I., Solheim, A., Andersen, E.S., Milliman, J., Mangerud, J., Hooke, R.LeB, 1995. Late Quaternary Sediment Yield from the High Arctic Svalbard Area. J. Geol. 103, 1–17. https://doi.org/10.1086/629718.

Emerson, S., Hedges, J.I., 1988. Processes controlling the organic carbon content of open ocean sediments. Paleoceanography 3, 621–634. https://doi.org/10.1029/PA003i005p00621.

Eynaud, F., Turon, J.L., Duprat, J., 2004. Comparison of the Holocene and Eemian palaeoenvironments in the South Icelandic Basin: dinoflagellate cysts as proxies for the North Atlantic surface circulation. Rev. Palaeobot. Palynol. Middle latitude dinoflagellates and their cysts 128, 55–79. https://doi.org/10.1016/S0034-6667(03)00112-X.

Ezat, M.M., Rasmussen, T.L., Groeneveld, J., 2014. Persistent intermediate water warming during cold stadials in the southeastern Nordic seas during the past 65 k.y. Geology 42, 663–666. https://doi.org/10.1130/G35579.1.

Fahl, K., Stein, R., 1997. Modern organic carbon deposition in the Laptev Sea and the adjacent continental slope: surface water productivity vs. terrigenous input. Org. Geochem. 26, 379–390. https://doi.org/10.1016/S0146-6380(97)00007-7.

Fensome, R.A., Williams, G.L., MacRae, R.A., 2019. The Lentin and Williams index of fossil dinoflagellates. American Association of Stratigraphic Palynologists Foundation 50.

Fronval, T., Jansen, E., 1997. Eemian and early Weichselian (140–60 ka) Paleoceanography and paleoclimate in the Nordic Seas with comparisons to Holocene conditions. Paleoceanography 12, 443–462. https://doi.org/10.1029/97PA00322.

Geibert, W., Matthiessen, J., Stimac, I., Wollenburg, J., Stein, R., 2021. Glacial episodes of a freshwater Arctic Ocean covered by a thick ice shelf. Nature 590, 97–102. https://doi.org/10.1038/s41586-021-03186-y.

Grøsfjeld, K., Funder, S., Seidenkrantz, M.-S., Glaister, C., 2006. Last Interglacial marine environments in the White Sea region, northwestern Russia. Boreas 35, 493–520. https://doi.org/10.1080/03009480600781917.

Guarino, M.-V., Sime, L.C., Schröeder, D., Malmierca-Vallet, I., Rosenblum, E., Ringer, M., Ridley, J., Feltham, D., Bitz, C., Steig, E.J., Wolff, E., Stroeve, J., Sellar, A., 2020. Sea-ice-free Arctic during the last Interglacial supports fast future loss. Nat. Clim. Chang. 10, 928–932. https://doi.org/10.1038/s41558-020-0865-2.

Haake, F.-W., Pflaumann, U., 1989. Late Pleistocene foraminiferal stratigraphy on the Vøring Plateau, Norwegian Sea. Boreas 18, 343–356. https://doi.org/10.1111/j.1502-3885.1989.tb00410.x.

Haine, T.W.N., Curry, B., Gerdes, R., Hansen, E., Karcher, M., Lee, C., Rudels, B., Spreen, G., de Steur, L., Stewart, K.D., Woodgate, R., 2015. Arctic freshwater export: Status, mechanisms, and prospects. Glob. Planet. Chang. 125, 13–35. https://doi.org/10.1016/j.gloplacha.2014.11.013.

Hall, A., 2004. The Role of Surface Albedo Feedback in climate. J. Clim. 17, 1550–1568.

Harland, R., 1983. Distribution maps of recent dinoflagellate cysts in bottom sediments from the North Atlantic Ocean and adjacent seas. Palaeontology 26, 321–387.

Hattermann, T., Isachsen, P.E., von Appen, W.-J., Albretsen, J., Sundfjord, A., 2016. Eddy-driven recirculation of Atlantic Water in Fram Strait. Geophys. Res. Lett. 43, 3406–3414. https://doi.org/10.1002/2016GL068323.

Head, M., 1996. Modern dinoflagellate cysts and their biological affinities, in American Association of Stratigraphic. Palynologists Foundation 3, 1197–1248.

Hebbeln, D., Wefer, G., 1997. Late Quaternary paleoceanography in the Fram Strait. Paleoceanography 12, 65–78. https://doi.org/10.1029/96PA02753.

Hennissen, J.A.I., Head, M.J., de Schepper, S., Groeneveld, J., 2017. Dinoflagellate cyst paleoecology during the plioceneepleistocene climatic transition in the North atlantic. Palaeogeogr. Palaeoclimatol. Palaeoecol. 470, 81e108. https://doi.org/10.1016/j.palaeo.2016.12.023.

Henrich, R., 1998. Dynamics of Atlantic water advection to the Norwegian-Greenland Sea — a time-slice record of carbonate distribution in the last 300 ky. Mar. Geol. 145, 95–131. https://doi.org/10.1016/S0025-3227(97)00103-5.

Heslop, D., De Schepper, S., Proske, U., 2011. Diagnosing the uncertainty of taxa relative abundances derived from count data. Mar. Micropaleontol. 79, 114–120. https://doi.org/10.1016/j.marmicro.2011.01.007.

Ingvaldsen, R.B., Assmann, K.M., Primicerio, R., Fossheim, M., Polyakov, I.V., Dolgov, A. V., 2021. Physical manifestations and ecological implications of Arctic Atlantification. Nat Rev Earth Environ 2, 874–889. https://doi.org/10.1038/s43017-021-00228-x.

Irvali, N., Ninnemann, U.S., Galaasen, E.V., Rosenthal, Y., Kroon, D., Oppo, D.W., Kleiven, H.F., Darling, K.F., Kissel, C., 2012. Rapid switches in subpolar North Atlantic hydrography and climate during the last Interglacial (MIS 5e). Paleoceanography 27. https://doi.org/10.1029/2011PA002244.

Irvali, N., Ninnemann, U.S., Kleiven, H., Kikki, F., Galaasen, E.V., Morley, A., Rosenthal, Y., 2016. Evidence for regional cooling, frontal advances, and East Greenland Ice Sheet changes during the demise of the last interglacial. Quat. Sci. Rev. 150, 184–199. https://doi.org/10.1016/j.quascirev.2016.08.029.

Ivanov, V.V., Alexeev, V.A., Repina, I., Koldunov, N.V., Smirnov, A., 2012. Tracing Atlantic Water Signature in the Arctic Sea Ice Cover East of Svalbard. Adv. Meteorol. 2012, e201818. https://doi.org/10.1155/2012/201818.

Jakobsson, M., Mayer, L., Coakley, B., Dowdeswell, J.A., Forbes, S., Fridman, B., Hodnesdal, H., Noormets, R., Pedersen, R., Rebesco, M., Schenke, H.W., Zarayskaya, Y., Accettella, D., Armstrong, A., Anderson, R.M., Bienhoff, P., Camerlenghi, A., Church, I., Edwards, M., Gardner, J.V., Hall, J.K., Hell, B., Hestvik, O., Kristoffersen, Y., Marcussen, C., Mohammad, R., Mosher, D., Nghiem, S. V., Pedrosa, M.T., Travaglini, P.G., Weatherall, P., 2012. The International Bathymetric Chart of the Arctic Ocean (IBCAO) Version 3.0. Geophys. Res. Lett. 39. https://doi.org/10.1029/2012GL052219.

Jakobsson, M., Nilsson, J., Anderson, L., Backman, J., Björk, G., Cronin, T.M., Kirchner, N., Koshurnikov, A., Mayer, L., Noormets, R., O'Regan, M., Stranne, C., Ananiev, R., Barrientos Macho, N., Cherniykh, D., Coxall, H., Eriksson, B., Flodén, T., Gemery, L., Gustafsson, Ö., Jerram, K., Johansson, C., Khortov, A., Mohammad, R., Semiletov, I., 2016. Evidence for an ice shelf covering the Central Arctic Ocean during the penultimate glaciation. Nat. Commun. 7, 10365. https://doi.org/10.1038/ncomms10365.

Jansen, E., Overpeck, J., Briffa, K.R., Duplessy, J.-C., Joos, F., Masson-Delmotte, V., Olago, D., Otto-Bliesner, B., Peltier, W.R., Rahmstorf, S., Ramesh, R., Raynaud, D., Rind, D., Solomina, O., Villalba, R., Zhang, D., 2007. Palaeoclimate. In: Solomon, S., Qin, D., Manning, M., Chen, Z., Marquis, M., Averyt, K.B., Tignor, M., Miller, H.L. (Eds.), Climate Change 2007: The Physical Science Basis. Contribution of Working Group I to the Fourth Assessment Report of the Intergovernmental Panel on Climate Change. Cambridge University Press, pp. 433–497.

Kellogg, T.B., Duplessy, J.C., Shackleton, N.J., 1978. Planktonic foraminiferal and oxygen isotopic stratigraphy and paleoclimatology of Norwegian Sea deep-sea cores. Boreas 7, 61–73. https://doi.org/10.1111/j.1502-3885.1978.tb00051.x.

Kissel, C., Laj, C., Labeyrie, L., Dokken, T., Voelker, A., Blamart, D., 1999. Rapid climatic variations during marine isotopic stage: 3. Magnetic analysis of sediments from Nordic Seas and North Atlantic. Earth Planet. Sci. Lett. 171, 489–502.

Knies, J., Stein, R., 1998. New aspects of organic carbon deposition and its paleoceanographic implications along the Northern Barents Sea margin during the last 30,000 years. Paleoceanography 13, 384–394. https://doi.org/10.1029/98PA01501.

Knies, J., Vogt, C., Stein, R., 1999. Late Quaternary growth and decay of the Svalbard/Barents Sea ice sheet and paleoceanographic evolution in the adjacent Arctic Ocean. Geo-Mar. Lett. 18, 195–202.

Kolling, H.M., Stein, R., Fahl, K., Sadatzki, H., de Vernal, A., Xiao, X., 2020. Biomarker Distributions in (Sub)-Arctic Surface Sediments and their potential for Sea Ice Reconstructions. Geochem. Geophys. Geosyst. 21, e2019GC008629. https://doi.org/10.1029/2019GC008629.

Köseoğlu, D., Belt, S.T., Knies, J., 2019. Abrupt shifts of productivity and sea ice regimes at the western Barents Sea slope from the last Glacial Maximum to the Bølling-Allerød interstadial. Quat. Sci. Rev. 222, 105903. https://doi.org/10.1016/j.quascirev.2019.105903.

Kremer, A., Stein, R., Fahl, K., Bauch, H., Mackensen, A., Niessen, F., 2018a. A 190-ka biomarker record revealing interactions between sea ice, Atlantic Water inflow and ice sheet activity in eastern Fram Strait. arktos 4, 22. https://doi.org/10.1007/s41063-018-0052-0.

Kremer, A., Stein, R., Fahl, K., Ji, Z., Yang, Z., Wiers, S., Matthiessen, J., Forwick, M., Löwemark, L., O'Regan, M., Chen, J., Snowball, I., 2018b. Changes in sea ice cover and ice sheet extent at the Yermak Plateau during the last 160 ka – Reconstructions from biomarker records. Quat. Sci. Rev. 182, 93–108. https://doi.org/10.1016/j.quascirev.2017.12.016.

Laskar, J., Robutel, P., Joutel, F., Gastineau, M., Correia, A.C.M., Levrard, B., 2004. A long-term numerical solution for the insolation quantities of the Earth. Astron. Astrophys. 428, 261–285. https://doi.org/10.1051/0004-6361:20041335.

Limoges, A., Ribeiro, S., Weckström, K., Heikkilä, M., Zamelczyk, K., Andersen, T.J., Tallberg, P., Massé, G., Rysgaard, S., Nørgaard-Pedersen, N., Seidenkrantz, M.-S., 2018a. Linking the Modern distribution of Biogenic Proxies in High Arctic Greenland Shelf Sediments to Sea Ice, primary production, and Arctic-Atlantic Inflow. J. Geophys. Res. Biogeosci. 123, 760–786. https://doi.org/10.1002/2017JG003840.

Limoges, A., Massé, G., Weckström, K., Poulin, M., Ellegaard, M., Heikkilä, M., Geilfus, N.-X., Sejr, M.K., Rysgaard, S., Ribeiro, S., 2018b. Spring Succession and Vertical Export of Diatoms and IP25 in a seasonally Ice-Covered High Arctic Fjord. Front. Earth Sci. 6. https://doi.org/10.3389/feart.2018.00226.

Lisiecki, L.E., Raymo, M.E., 2005. A Pliocene-Pleistocene stack of 57 globally distributed benthic 18O records. Paleoceanography 20 (1). https://doi.org/10.1029/2004PA001071.

Locarnini, R.A., Mishonov, A.V., Baranova, O.K., Boyer, T.P., Zweng, M.M., Garcia, H.E., Reagan, J.R., Seidov, D., Weathers, K., Paver, C.R., Smolyar, I., 2019. In: Mishonov Technical, A. (Ed.), World Ocean Atlas 2018, Volume 1: Temperature, NOAA Atlas NESDIS, vol. 81, p. 52pp.

Mangerud, J., Jansen, E., Landvik, J.Y., 1996. Late Cenozoic history of the Scandinavian and Barents Sea ice sheets. Glob. Planet. 12, 11–26. https://doi.org/10.1016/0921-8181(95)00009-7.

Mangerud, J., Dokken, T., Hebbeln, D., Heggen, B., Ingólfsson, Ó., Landvik, J.Y., Mejdahl, V., Svendsen, J.I., Vorren, T.O., 1998. Fluctuations of the Svalbard–Barents Sea Ice Sheet during the last 150 000 years. Quat. Sci. Rev. 17, 11–42. https://doi.org/10.1016/S0277-3791(97)00069-3.

Manley, T.O., 1995. Branching of Atlantic Water within the Greenland-Spitsbergen Passage: an estimate of recirculation. J. Geophys. Res. Oceans 100, 20627–20634. https://doi.org/10.1029/95JC01251.

Marret, F., Zonneveld, K.A.F., 2003. Atlas of modern organic-walled dinoflagellate cyst distribution. Rev. Palaeobot. Palynol. 125, 1–200. https://doi.org/10.1016/S0034-6667(02)00229-4.
Marret, F., Eiriksson, J, Knudsen, K.L., Turon, J.-L., Scourse, J.D., 2004. Distribution of dinoflagellate cyst assemblages in surface sediments from the northern and western shelf of Iceland. Rev. Palaeobot. Palynol. Middle latitude dinoflagellates and their cysts 128, 35–53. https://doi.org/10.1016/S0034-6667(03)00111-8.
Matthiessen, J., Knies, J., 2001. Dinoflagellate cyst evidence for warm interglacial conditions at the northern Barents Sea margin during marine oxygen isotope stage 5. J. Quat. Sci. 16, 727–737. https://doi.org/10.1002/jqs.656.
Matthiessen, J., Knies, J., Nowaczyk, N.R., Stein, R., 2001. Late Quaternary dinoflagellate cyst stratigraphy at the Eurasian continental margin, Arctic Ocean: indications for Atlantic water inflow in the past 150,000 years. Glob. In: Planet. Change, The late Quaternary stratigraphy and environments of northern Eurasia and the adjacent Arctic seas - new contributions from QUEEN, 31, pp. 65–86. https://doi.org/10.1016/S0921-8181(01)00113-8.
Matthiessen, J., de Vernal, A., Head, M., Okolodkov, Y., Zonneveld, K., Harland, R., 2005. Modern organic-walled dinoflagellate cysts in arctic marine environments and their (paleo-) environmental significance. Paläontol. Z. 79, 3–51. https://doi.org/10.1007/BF03021752.
Mokeddem, Z., McManus, J.F., Oppo, D.W., 2014. Oceanographic dynamics and the end of the last interglacial in the subpolar North Atlantic. Proc. Natl. Acad. Sci. 111, 11263–11268. https://doi.org/10.1073/pnas.1322103111.
Müller, J., Massé, G., Stein, R., Belt, S.T., 2009. Variability of sea-ice conditions in the Fram Strait over the past 30,000 years. Nat. Geosci. 2, 772–776. https://doi.org/10.1038/ngeo665.
Müller, J., Wagner, A., Fahl, K., Stein, R., Prange, M., Lohmann, G., 2011. Towards quantitative sea ice reconstructions in the northern North Atlantic: a combined biomarker and numerical modelling approach. Earth Planet. Sci. Lett. 306, 137–148. https://doi.org/10.1016/j.epsl.2011.04.011.
Müller, J., Werner, K., Stein, R., Fahl, K., Moros, M., Jansen, E., 2012. Holocene cooling culminates in sea ice oscillations in Fram Strait. Quat. Sci. Rev. 47, 1–14. https://doi.org/10.1016/j.quascirev.2012.04.024.
Nelson, D.M., Smith, W.O., Muench, R.D., Gordon, L.I., Sullivan, C.W., Husby, D.M., 1989. Particulate matter and nutrient distributions in the ice-edge zone of the Weddell Sea: relationship to hydrography during late summer. Deep Sea Res. Part Oceanogr. Res. Pap. 36, 191–209. https://doi.org/10.1016/0198-0149(89)90133-7.
ngrip community members, 2004. High-resolution record of Northern Hemisphere climate extending into the last interglacial period. Nature 431, 147–151.
Nørgaard-Pedersen, N., Spielhagen, R.F., Erlenkeuser, H., Grootes, P.M., Heinemeier, J., Knies, J., 2003. Arctic Ocean during the last Glacial Maximum: Atlantic and polar domains of surface water mass distribution and ice cover. Paleoceanography 18. https://doi.org/10.1029/2002PA000781.
Notz, D., Stroeve, J., 2016. Observed Arctic Sea-ice loss directly follows anthropogenic CO_2 emission. Science 354, 747–750. https://doi.org/10.1126/science.aag2345.
Notz, D., Stroeve, J., 2018. The Trajectory Towards a seasonally Ice-Free Arctic Ocean. Curr. Clim. Chang. Rep. 4, 407–416. https://doi.org/10.1007/s40641-018-0113-2.
Onarheim, I.H., Smedsrud, L.H., Ingvaldsen, R.B., Nilsen, F., 2014. Loss of sea ice during winter north of Svalbard, 66, p. 23933. https://doi.org/10.3402/tellusa.v66.23933.
Penaud, A., Eynaud, F., Turon, J.L., Zaragosi, S., Marret, F., Bourillet, J.F., 2008. Interglacial variability (MIS 5 and MIS 7) and dinoflagellate cyst assemblages in the Bay of Biscay (North Atlantic). Mar. Micropaleontol. 68, 136–155. https://doi.org/10.1016/j.marmicro.2008.01.007.
Polyakov, I.V., Pnyushkov, A.V., Alkire, M.B., Ashik, I.M., Baumann, T.M., Carmack, E. C., Goszczko, I., Guthrie, J., Ivanov, V.V., Kanzow, T., Krishfield, R., Kwok, R., Sundfjord, A., Morison, J., Rember, R., Yulin, A., 2017. Greater role for Atlantic inflows on sea-ice loss in the Eurasian Basin of the Arctic Ocean. Science 356, 285–291. https://doi.org/10.1126/science.aai8204.
Railsback, L.B., Gibbard, P.L., Head, M.J., Voarintsoa, N.R.G., Toucanne, S., 2015. An optimized scheme of lettered marine isotope substages for the last 1.0 million years, and the climatostratigraphic nature of isotope stages and substages. Quat. Sci. Rev. 111, 94–106. https://doi.org/10.1016/j.quascirev.2015.01.012.
Rasmussen, T.L., Oppo, D.W., Thomsen, E., Lehman, S.J., 2003a. Deep sea records from the Southeast Labrador Sea: Ocean circulation changes and ice-rafting events during the last 160,000 years. Paleoceanography 18. https://doi.org/10.1029/2001PA000736.
Rasmussen, T.L., Thomsen, E., Kuijpers, A., Wastegård, S., 2003b. Late warming and early cooling of the sea surface in the Nordic seas during MIS 5e (Eemian Interglacial). Quat. Sci. Rev. 22, 809–821. https://doi.org/10.1016/S0277-3791(02)00254-8.
Rasmussen, T.L., Thomsen, E., Ślubowska, M.A., Jessen, S., Solheim, A., Koç, N., 2007. Paleoceanographic evolution of the SW Svalbard margin (76°N) since 20,000 14C yr BP. Quat. Res. 67, 100–114. https://doi.org/10.1016/j.yqres.2006.07.002.
Reigstad, M., Wassmann, P., Wexels Riser, C., Øygarden, S., Rey, F., 2002. Variations in hydrography, nutrients and chlorophyll a in the marginal ice-zone and the Central Barents Sea. Journal of Marine Systems, Seasonal C-cycling variability in the open and ice-covered waters of the Barents Sea 38, 9–29. https://doi.org/10.1016/S0924-7963(02)00167-7.
Rimbu, N., Lohmann, G., Kim, J.-H., Arz, H.W., Schneider, R., 2003. Arctic/North Atlantic Oscillation signature in Holocene Sea surface temperature trends as obtained from alkenone data. Geophys. Res. Lett. 30. https://doi.org/10.1029/2002GL016570.
Risebrobakken, B., Dokken, T., Jansen, E., 2005. Extent and Variability of the Meridional Atlantic Circulation in the Eastern Nordic Seas during Marine Isotope stage 5 and its Influence on the Inception of the last Glacial. In: The Nordic Seas: An Integrated Perspective. American Geophysical Union (AGU), pp. 323–339. https://doi.org/10.1029/158GM20.
Risebrobakken, B., Balbon, E., Dokken, T., Jansen, E., Kissel, C., Labeyrie, L., Richter, T., Senneset, L., 2006. The penultimate deglaciation: High-resolution paleoceanographic evidence from a north–south transect along the eastern Nordic Seas. Earth Planet. Sci. Lett. 241, 505–516. https://doi.org/10.1016/j.epsl.2005.11.032.
Risebrobakken, B., Dokken, T., Otterå, O.H., Jansen, E., Gao, Y., Drange, H., 2007. Inception of the northern European ice sheet due to contrasting ocean and insolation forcing. Quat. Res. 67, 128–135. https://doi.org/10.1016/j.yqres.2006.07.007.
Risebrobakken, B., Dokken, T., Smedsrud, L.H., Andersson, C., Jansen, E., Moros, M., Ivanova, E.V., 2011. Early Holocene temperature variability in the Nordic Seas: the role of oceanic heat advection versus changes in orbital forcing. Paleoceanography 26. https://doi.org/10.1029/2011PA002117.
Robinson, N., Eglinton, G., Brassell, S.C., Cranwell, P.A., 1984. Dinoflagellate origin for sedimentary 4α-methylsteroids and 5α(H)-stanols. Nature 308, 439–442. https://doi.org/10.1038/308439a0.
Rochon, A., de Vernal, A., Turon, J.-L., Head, M.J., 1999. Distribution of recent dinoflagellate cysts in surface sediments from the North Atlantic and adjacent seas in relation to sea-surface parameters. Am. Assoc. Stratigr. Palynol. Contrib. Ser. 35, 1–146.
Ruddiman, W.F., Molfino, B., Esmay, A., Porkas, E., 1980. Evidence bearing on the mechanism of rapid deglaciation. Clim. Chang. 3, 65–87.
Rudels, B., Fahrbach, E., Meincke, J., Budéus, G., Eriksson, P., 2002. The East Greenland current and its contribution to the Denmark Strait overflow. ICES J. Mar. Sci. 59, 1133–1154. https://doi.org/10.1006/jmsc.2002.1284.
Sakshaug, E., 2004. Primary and secondary production in the Arctic seas. In: Stein, R., Macdonald, R.W. (Eds.), The Organic Carbon Cycle in the Arctic Ocean. Springer, Berlin, pp. 57e82.
Sánchez Goñi, M.F., Eynaud, F., Turon, J.L., Shackleton, N.J., 1999. High resolution palynological record off the Iberian margin: direct land-sea correlation for the last Interglacial complex. Earth Planet. Sci. Lett. 171, 123–137. https://doi.org/10.1016/S0012-821X(99)00141-7.
Schauer, U., Fahrbach, E., Osterhus, S., Rohardt, G., 2004. Arctic warming through the Fram Strait: Oceanic heat transport from 3 years of measurements. J. Geophys. Res. Oceans 109. https://doi.org/10.1029/2003JC001823.
Schlitzer, R., 2023. Ocean Data View.
Shackleton, N., Chapman, M., Sanchez Goñi, M., Pailler, D., Lancelot, Y., 2002. The Classic Marine Isotope Substage 5e. Quat. Res. 58, 14–16. https://doi.org/10.1006/qres.2001.2312.
Shackleton, N.J., Sánchez-Goñi, M.F., Pailler, D., Lancelot, Y., 2003. Marine Isotope Substage 5e and the Eemian Interglacial. Glob. Planet. Chang. 36, 151–155. https://doi.org/10.1016/S0921-8181(02)00181-9.
Spielhagen, R.F., Baumann, K.-H., Erlenkeuser, H., Nowaczyk, N.R., Nørgaard-Pedersen, N., Vogt, C., Weiel, D., 2004. Arctic Ocean deep-sea record of northern Eurasian ice sheet history. Quat. Sci. Rev. Quaternary Environments of the Eurasian North (QUEEN) 23, 1455–1483. https://doi.org/10.1016/j.quascirev.2003.12.015.
Stein, R., Boucsein, B., Fahl, K., Garcia de Oteyza, T., Knies, J., Niessen, F., 2001. Accumulation of particulate organic carbon at the Eurasian continental margin during late Quaternary times: controlling mechanisms and paleoenvironmental significance. Glob. Planet. Chang. 31, 87–104. https://doi.org/10.1016/S0921-8181(01)00114-X.
Stein, R., Fahl, K., Müller, J., 2012. Proxy reconstruction of Arctic Ocean sea ice history - from IRD to IP25. Polarforschung 82, 37–71.
Stein, R., Fahl, K., Schreck, M., Knorr, G., Niessen, F., Forwick, M., Gebhardt, C., Jensen, L., Kaminski, M., Kopf, A., Matthiessen, J., Jokat, W., Lohmann, G., 2016. Evidence for ice-free summers in the late Miocene Central Arctic Ocean. Nat. Commun. 7, 1–13. https://doi.org/10.1038/ncomms11148.
Stein, R., Fahl, K., Gierz, P., Niessen, F., Lohmann, G., 2017. Arctic Ocean sea ice cover during the penultimate glacial and the last interglacial. Nat. Commun. 8, 1–13. https://doi.org/10.1038/s41467-017-00552-1.
Stein, R., Kremer, A., Fahl, K., 2022. Past glacial-interglacial changes in Arctic Ocean sea-ice conditions. Past Glob. Chang. Mag. 30, 90–91. https://doi.org/10.22498/pages.30.2.90.
Steinsland, K., Grant, D.M., Ninnemann, U.S., Fahl, K., Stein, R., De Schepper, S., 2023. Sea ice variability in the North Atlantic subpolar gyre throughout the last Interglacial. Quat. Sci. Rev. 313, 108198. https://doi.org/10.1016/j.quascirev.2023.108198.
Steinsland, Kristine; Grant, Danielle; Fahl, Kirsten; Stein, Ruediger; Rasmussen, Tine L; Ninnemann, Ulysses S; Knies, Jochen; Velle, Julie Heggdal; De Schepper, Stijn (2025): Multiproxy data from sediment core CAGE19-3-KH14-GPC02 between 140 and 90 ka [dataset bundled publication]. PANGAEA, https://doi.org/10.1594/PANGAEA.973596.
Steinsund, P.I., Hald, M., 1994. Recent calcium carbonate dissolution in the Barents Sea: Paleoceanographic applications. Mar. Geol. 117, 303–316. https://doi.org/10.1016/0025-3227(94)90022-1.
Stockmarr, J., 1971. Tablets with spores used in absolute pollen analysis. Pollen Spores 13, 615e621.
Stroeve, J., Holland, M.M., Meier, W., Scambos, T., Serreze, M., 2007. Arctic Sea ice decline: Faster than forecast. Geophys. Res. Lett. 34. https://doi.org/10.1029/2007GL029703.
Stroeve, J.C., Serreze, M.C., Holland, M.M., Kay, J.E., Malanik, J., Barrett, A.P., 2012. The Arctic's rapidly shrinking sea ice cover: a research synthesis. Clim. Chang. 110, 1005–1027. https://doi.org/10.1007/s10584-011-0101-1.
Svendsen, J.I., Alexanderson, H., Astakhov, V.I., Demidov, I., Dowdeswell, J.A., Funder, S., Gataullin, V., Henriksen, M., Hjort, C., Houmark-Nielsen, M.,

Hubberten, H.W., Ingólfsson, Ó., Jakobsson, M., Kjær, K.H., Larsen, E., Lokrantz, H., Lunkka, J.P., Lyså, A., Mangerud, J., Matiouchkov, A., Murray, A., Möller, P., Niessen, F., Nikolskaya, O., Polyak, L., Saarnisto, M., Siegert, C., Siegert, M.J., Spielhagen, R.F., Stein, R., 2004. Late Quaternary ice sheet history of northern Eurasia. Quat. Sci. Rev. 23, 1229–1271. https://doi.org/10.1016/j.quascirev.2003.12.008.

Thibodeau, B., Bauch, H.A., Pedersen, T.F., 2017. Stratification-induced variations in nutrient utilization in the Polar North Atlantic during past interglacials. Earth Planet. Sci. Lett. 457, 127–135. https://doi.org/10.1016/j.epsl.2016.09.060.

Van Nieuwenhove, N., Bauch, H.A., Matthiessen, J., 2008. Last interglacial surface water conditions in the eastern Nordic Seas inferred from dinocyst and foraminiferal assemblages. Mar. Micropaleontol. 66, 247–263. https://doi.org/10.1016/j.marmicro.2007.10.004.

Van Nieuwenhove, N., Bauch, H.A., Eynaud, F., Kandiano, E., Cortijo, E., Turon, J.-L., 2011. Evidence for delayed poleward expansion of North Atlantic surface waters during the last interglacial (MIS 5e). Quat. Sci. Rev. 30, 934–946. https://doi.org/10.1016/j.quascirev.2011.01.013.

Van Nieuwenhove, N., Head, M.J., Limoges, A., Pospelova, V., Mertens, K.N., Matthiessen, J., De Schepper, S., de Vernal, A., Eynaud, F., Londeix, L., Marret, F., Penaud, A., Radi, T., Rochon, A., 2020. An overview and brief description of common marine organic-walled dinoflagellate cyst taxa occurring in surface sediments of the Northern Hemisphere. Marine Micropaleontology, Taxonomy and distribution of modern organic-walled dinoflagellate cysts in surface sediments from the Northern Hemisphere: an update of Rochon et al., 1999, 159, p. 101814. https://doi.org/10.1016/j.marmicro.2019.101814.

Vancoppenolle, M., Meiners, K.M., Michel, C., Bopp, L., Brabant, F., Carnat, G., Delille, B., Lannuzel, D., Madec, G., Moreau, S., Tison, J.-L., van der Merwe, P., 2013. Role of sea ice in global biogeochemical cycles: emerging views and challenges. Quaternary Science Reviews, Sea Ice in the Paleoclimate System: the Challenge of Reconstructing Sea Ice from. Proxies 79, 207–230. https://doi.org/10.1016/j.quascirev.2013.04.011.

Vasskog, K., Langebroek, P.M., Andrews, J.T., Nilsen, J.E.Ø., Nesje, A., 2015. The Greenland Ice Sheet during the last glacial cycle: current ice loss and contribution to sea-level rise from a palaeoclimatic perspective. Earth Sci. Rev. 150, 45–67. https://doi.org/10.1016/j.earscirev.2015.07.006.

Vermassen, F., O'Regan, M., de Boer, A., Schenk, F., Razmjooei, M., West, G., Cronin, T. M., Jakobsson, M., Coxall, H.K., 2023. A seasonally ice-free Arctic Ocean during the last Interglacial. Nat. Geosci. 16, 723–729. https://doi.org/10.1038/s41561-023-01227-x.

Vinje, T., 2001. Fram Strait Ice Fluxes and Atmospheric Circulation: 1950–2000. J. Clim. 14, 3508–3517. https://doi.org/10.1175/1520-0442(2001)014<3508:FSIFAA>2.0.CO;2.

Vogt, C., Knies, J., Spielhagen, R.F., Stein, R., 2001. Detailed mineralogical evidence for two nearly identical glacial/deglacial cycles and Atlantic water advection to the Arctic Ocean during the last 90,000 years. Glob. Planet. Chang. 31, 23–44. https://doi.org/10.1016/S0921-8181(01)00111-4.

Volkman, J.K., 1986. A review of sterol markers for marine and terrigenous organic matter. Org. Geochem. 9, 83–99. https://doi.org/10.1016/0146-6380(86)90089-6.

Volkman, J.K., Barrett, S.M., Blackburn, S.I., Mansour, M.P., Sikes, E.L., Gelin, F., 1998. Microalgal biomarkers: a review of recent research developments. Org. Geochem. 29, 1163–1179. https://doi.org/10.1016/S0146-6380(98)00062-X.

Walczowski, W., Piechura, J., 2011. Influence of the West Spitsbergen current on the local climate. Int. J. Climatol. 31, 1088–1093. https://doi.org/10.1002/joc.2338.

Wall, D., Dale, B., 1966. Living fossils" in western atlantic plankton. Nature 211, 1025e1026. https://doi.org/10.1038/2111025a0.

Werner, K., Müller, J., Husum, K., Spielhagen, R.F., Kandiano, E.S., Polyak, L., 2016. Holocene Sea subsurface and surface water masses in the Fram Strait – Comparisons of temperature and sea-ice reconstructions. Quat. Sci. Rev. 147, 194–209. https://doi.org/10.1016/j.quascirev.2015.09.007. Special Issue: PAST Gateways (Palaeo-Arctic Spatial and Temporal Gateways).

Winkelmann, D., Schäfer, C., Stein, R., Mackensen, A., 2008. Terrigenous events and climate history of the Sophia Basin. Arctic Ocean. Geochem. Geophys. Geosystems 9. https://doi.org/10.1029/2008GC002038.

Xiao, X., Fahl, K., Müller, J., Stein, R., 2015. Sea-ice distribution in the modern Arctic Ocean: Biomarker records from trans-Arctic Ocean surface sediments. Geochim. Cosmochim. Acta 155, 16–29. https://doi.org/10.1016/j.gca.2015.01.029.

Xiao, W., Polyak, L., Wang, R., Löwemark, L., Mei, J., You, D., Wang, W., Wu, L., Jin, X., 2020. Middle to late Pleistocene Arctic paleoceanographic changes based on sedimentary records from Mendeleev Ridge and Makarov Basin. Quat. Sci. Rev. 228, 106105. https://doi.org/10.1016/j.quascirev.2019.106105.

You, D., Stein, R., Fahl, K., Williams, M.C., Schmidt, D.N., McCave, I.N., Barker, S., Schefuß, E., Niu, L., Kuhn, G., Niessen, F., 2023. Last deglacial abrupt climate changes caused by meltwater pulses in the Labrador Sea. Commun. Earth Environ. 4, 1–12. https://doi.org/10.1038/s43247-023-00743-3.

Zamelczyk, K., Rasmussen, T.L., Husum, K., Godtliebsen, F., Hald, M., 2014. Surface water conditions and calcium carbonate preservation in the Fram Strait during marine isotope stage 2, 28.8–15.4 kyr. Paleoceanography 29, 1–12. https://doi.org/10.1002/2012PA002448.

Zhuravleva, A., Bauch, H.A., Spielhagen, R.F., 2017. Atlantic water heat transfer through the Arctic Gateway (Fram Strait) during the last Interglacial. Glob. Planet. Chang. 157, 232–243. https://doi.org/10.1016/j.gloplacha.2017.09.005.

Zonneveld, K.A.F., Marret, F., Versteegh, G.J.M., Bogus, K., Bonnet, S., Bouimetarhan, I., Crouch, E., de Vernal, A., Elshanawany, R., Edwards, L., Esper, O., Forke, S., Grøsfjeld, K., Henry, M., Holzwarth, U., Kielt, J.-F., Kim, S.-Y., Ladouceur, S., Ledu, D., Chen, L., Limoges, A., Londeix, L., Lu, S.-H., Mahmoud, M.S., Marino, G., Matsouka, K., Matthiessen, J., Mildenhal, D.C., Mudie, P., Neil, H.L., Pospelova, V., Qi, Y., Radi, T., Richerol, T., Rochon, A., Sangiorgi, F., Solignac, S., Turon, J.-L., Verleye, T., Wang, Y., Wang, Z., Young, M., 2013. Atlas of modern dinoflagellate cyst distribution based on 2405 data points. Rev. Palaeobot. Palynol. 191, 1–197. https://doi.org/10.1016/j.revpalbo.2012.08.003.